Ca' Foscari
University
of Venice

Single Cycle Degree programme

in Science and Technology
of Bio and Nanomaterials
"DM 270/04"

Final Thesis

Mesoporous zirconia nanoparticles for biomedical applications

Characterization, functionalization and case studies as antibiofouling agent

Supervisor
Ch. Prof. Pietro Riello

Assistant supervisor
PhD Emmanuele Ambrosi

Graduand
Benedetta Leonetti
Matriculation Number 851554

Academic Year
2015/ 2016

INDEX

Abbreviations

APS-MSNs: APTES – mesoporous silica nanoparticles

APTES: 3-(aminopropyl)triethoxysilane

BDDT: Brunauer-Deming-Deming-Teller

BET: Brunauer–Emmett–Teller

BJH: Barret-Joyner-Halenda

$CaCl_2$: calcium chloride

CAPS: 3-(cycloexilamine)-1-propanesulfonic acid

CLSM: confocal laser scanning microscopy

CTAB: cetytrimethylammonium bromide

DDSs: drug delivery systems

DLS: dynamic light scattering

DRIFT: diffuse reflectance infrared Fourier transform

DSC: differential scanning calorimetry

EPS: exopolysaccharides

FT-IR: Fourier transform infrared

EtOH: ethanol

HAp: hydroxyapatite

HCl: hydrochloric acid

HDMS: hexamethyldisilazane

K_3PO_4: potassium chloride

MBC: minimal biocidal concentration

MBEC: minimal biofilm eradication concentration

MIC: minimal inhibitory concentration

MRSA: methicillin-resistant *Staphylococcus aureus*

MSSA: methicillin-susceptible *Staphylococcus aureus*

MSA: mannitol salt agar

MSCs: mesenchymal stem cells

MSNs: mesoporous silica nanoparticles

MWCO: molecular weight cut-off

MZNs: mesoporous zirconia nanoparticles

NA: nutrient agar

NB: nutrient broth

$Na_3C_6H_5O_7$: sodium citrate

NaF: sodium fluoride

Na_3PO_4: sodium phosphate

NPs: nanoparticles

PBS: phosphate buffered saline

R6G: rhodamine 6G

ROS: reacting oxygen species

SEM: scanning electron microscope

TEM: transmission electron microscope

TGA: thermogravimetric analyses

TSA: tryptic soy agar

TSB: tryptic soy broth

VCN: Vancomycin

VISA: vancomycin-intermediate *S. aureus*

VRSA: vancomycin-resistant *S. aureus*

XRPD: X-ray powder diffraction

ZP: zeta potential

$Zr(OPr)_4$: zirconium(IV) propoxide

1 Introduction

1.1 Nanotechnology

The milestone of science of materials in last few decades is certainly nanotechnology, because of its wide range of applications in the most various fields, spanning from medicine to agriculture, food storage, food packaging, nanosensors, and environmental biotechnology. This versatility is due both to the opportunity to involve biomolecules in the engineered systems and to the special properties of nanomaterials, whose properties change from the bulk materials. During these last years there were more and more definitions of nanomaterials, since when R. Feynmann[1] gave one of his most famous lessons, saying "There's plenty of room at the bottom" in 1959 at California Institute of Technology, introducing the possibility to manipulate matter at an atomic level and trying to revolutionise the chemistry. Currently the most used definition of nanotechnology is the science dealing with objects and structures with at least one of the dimensions ranging between 1 to 100 nm, even if there are some exceptions. For instance, in the pharmaceutical or cosmetics area the size limitation is not so important because of bioavailability, reduced toxicity, lower and controlled dose, solubility and other advantages can be reached even by systems larger than 100 nm[2]. Nanoparticles and nanopowders which can be produced in suspensions (colloids), sol-gel, aerosols etc., offer a wide range of new and improved products. As the size of the material is reduced, reaching nanoscale regime, new properties can be obtained[3]. Nanostructured systems have different properties compared to bulk counterparts. Even if size is not usually mentioned as key factor, properties of materials can be size-dependent. Nanomaterials are intermediate in size between single atoms or molecules and bulk materials, so they don't follow Newtonian physics, but quantum mechanics. Therefore, nanoscience deals with supramolecular chemistry, so hydrogen and Van der Waals bonding and also hydrophobic effect have a key role in the interactions between molecules[3]. Smaller particles have larger active surfaces per unit of volume and mass[4]. This is due to the high surface-to-volume ratio and the high surface energy. These properties could also be improved by porosity. Nanostructures have a significant proportion of atoms on the surface and this is crucial for catalysis reactions, detection activity, physical adsorption, etc. This depends on the inverse proportionality between surface area and radius of materials. For this reason, nanotechnologies

have peculiar properties, more different than bulk materials, as exceptional electrical, optical and mechanical properties, that could also open the way to the so-called nanomedicine[3].

1.2 Nanomedicine

Nanomedicine is the application of nanotechnology to health and medicine and it's usually synonymous of nanobiotechnology, considering health as applied biology[1,5].

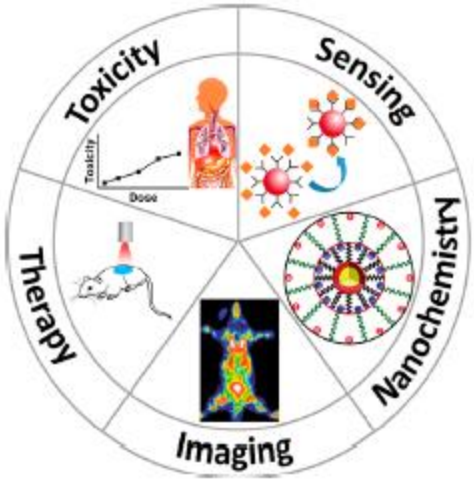

Figure 1.1 Nanomedicine fields of application[5] (Chen et al. 2016)

Microengineering and nanotechnology developments will lead to major benefits in bio-medical applications, through the integration of mechanical, optical, electronic and fluidic components produced in bio-compatible materials. Some examples are minimally invasive surgery, accurate and efficient drug targeting and delivery, innovations in diagnostics and imaging, improved adhesion growth of living tissue cells on to prosthetic implants by micro- and nano- surface patterning of implant materials. Actually, more biocompatible materials and surfaces are already being designed and tested. These systems demonstrate a remarkable ability to arrive at targeted sites, as a specific organ, tissue, or even underlying cell, in enormously larger concentrations than normal. In effect, these medicinal 'bullets' coated with antibodies can resist to attacks by the body's own defence cells, avoiding the release of toxic drugs on to healthy tissue[4,5].

About applied medicine, the main fields of application of these systems are drug delivery and regenerative medicine. Some devices have characteristics for both of them.

Biomaterials are natural or artificial substances employed to treat, replace or improve a tissue or an organ. They are classified for their origin or for their composition. The Science of

Biomaterials studies their interaction with the human body, since no biomaterial is completely inert in a body, so they can be classified also referring to the effects they have on the organism and vice versa. It's very important underline that they are in contact with biological fluids and this interaction should not be harmful for the patient. In other terms, biocompatibility is the first requirement for a biomaterial and depends on its physicochemical properties. Examples of biomaterials are that used for orthopaedic devices, cardiac, dental or for soft tissues implants, surgical instruments and, in the last few years also biological tissues and nanotechnologies[6,7].

1.2.1 Drug delivery systems (DDSs)

Drug delivery is the incorporation of a drug within structured carriers via encapsulation, absorption, adsorption, or conjugation, for safe and stable administration in the body. DDSs and, in particular, nano-DDSs (nano-drug delivery systems) should enhance delivery by active or passive targeting, can control release at target sites and overcome the multidrug resistance exhibited by each type of diseased cells. These systems allow incorporation of different types of drugs for combination therapy of complex diseases, where a single drug is not enough. This avoids also all secondary side effects of toxicity, increasing targeting efficiency with a lower dose, and, at the same time, preserving the high drug bioavailability. Hydrophobic, hydrophilic, small or macromolecular drugs, such as peptides, proteins, and DNA, can be carried[5,8,9].

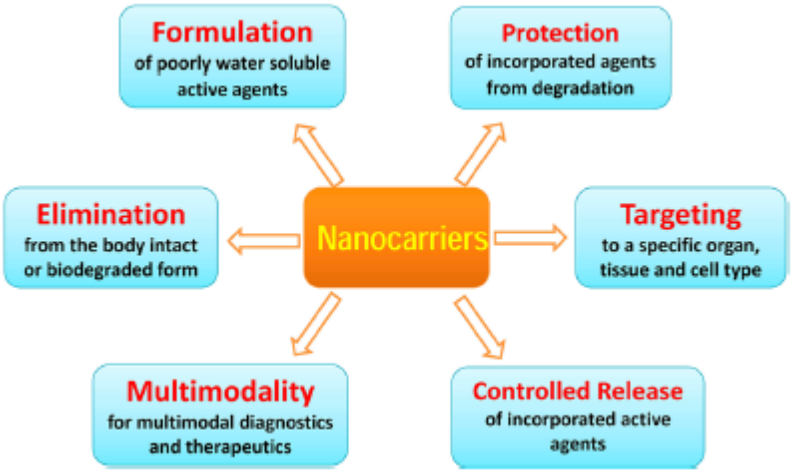

Figure 1.2 DDS main properties and advantages[5] (Chen et al. 2016)

Examples of carriers are micelles, dendrimers, carbon nanotubes, lyposomes, polymeric carriers, inorganic nanoparticles, such as quantum dots, gold or iron oxide nanoparticles and

mesoporous nanoparticles[2]. They include structures with internal pores and channels which can be used to host drug molecules. Mesoporous silica nanoparticles (MSNs) and large porous silicon nanoparticles are prominent examples of this, because of their biocompatibility and flexibility.

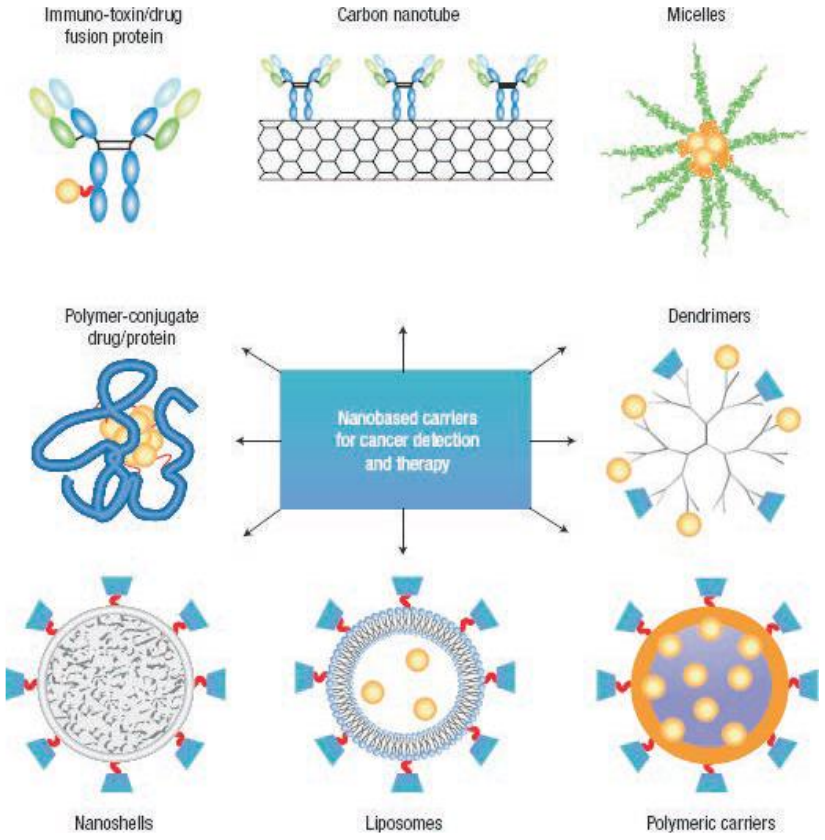

Figure 1.3 Most used nanocarriers in medicine[2] (Bawa et al. 2016)

This permits a tailored design, since it is possible to control their size, shape, porosity, and both internal and external surface functionalization. These variables affect particles behaviour under biological conditions and give the possibility to make the system stealth and thus able to escape from any immune response[9]. Nano-DDSs are also defined as smart systems, because they can release drugs in different ways or different times under determined stimuli. These can be exogenous, such as ultrasound, magnetic field and light, or endogenous, such as pH, enzymes, ionic strength etc[8]. Despite this, organic formulation need more progress into the clinical trial arena[5].

1.2.2 Regenerative medicine

Nanobiomaterials provide a new platform for the therapeutic reconstruction and engineering of tissues and organs and regenerative therapies, including implants to repair or replace damaged tissues or complete organs, using all biological, chemical, structural, physiological and functional properties of nanostructured systems. However, the nanobio-devices should be designed to interact with the cellular components without altering their regular biological activities. They should be biocompatible, non-toxic and biodegradable. There are two types of systems: soft and hard tissues. Soft tissues generally require both synthetic and biosynthesized polymers. Hard tissue engineering is related to hybrid systems where the inorganic compounds play a crucial role in the structure and function. This requires composites, a mixture of two or more materials (like synthetic or natural polymers) with markedly different physical or chemical properties.

A better knowledge of stem cells and their differentiation and signalling combined with the input of nanotechnologies are providing the basis for the development of new strategies in these therapies, trying to manipulate these cells with nanotechnologies. In this case, scaffolds play a key role to transport substances from and to the cells and as communication network. For example, an area of particular interest in nanomedicine is bone repair. However, bone repair and regeneration are extremely complex processes because they require a suitable scaffold and a 3D-structure, proper osteoconductive signals and growth factors, etc. Many materials such as ceramics, alloys, glasses, polymers and biopolymers have been tested[9].

Two biomaterials largely used in medicine are zirconium(IV) oxide (ZrO_2) and hydroxyapatite ($Ca_5(PO_4)_3OH$), both in orthopaedics and dentistry.

1.3 Zirconium(IV) oxide nanoparticles

Zirconium oxide is an interesting ceramic biomaterial, because it could offer some advantages such as biocompatibility and chemical inertia, suitable properties for *in vivo* biomedical application and drug loading processes.

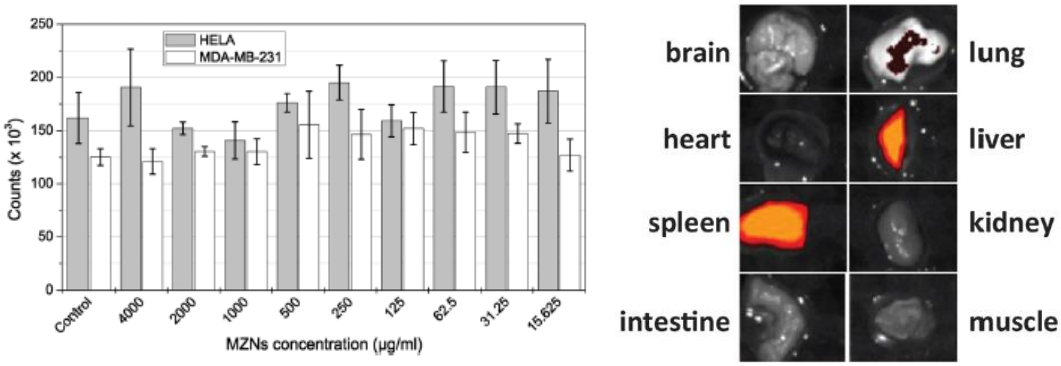

Figure 1.4 Preliminary studies of biocompatibility of MZNs. On the left: tumoral cells viability assay doesn't show relevant differences between treated and untreated cells with NPs. On the right: *in vivo* biodistribution of MZNs (orange areas). They mostly accumulate in spleen and liver as other known NPs[10] (Sponchia et al. 2015).

Typical applications of the bulk material are in orthopaedics or dentistry, such as bone or dental implants, especially with the use of stabilizing agents, which can improve its resistance to fractures. For its mechanical properties, which are very similar to those of metals, it was called "ceramic steel" by Garvie in1975. In the last few decades, great attention has been dedicated to the nanoscaled counterpart. In fact, the possibility to obtain a system with high surface area, good chemical stability, higher than alumina or silica, amphoteric and redox properties, is fascinating and opens the way to more and more applications. However, the reaction to produce pure zirconium(IV) oxide nanosystems with the appropriate structural characteristics of a good nanocarrier is not so simple, especially with a spherical shape with a well-defined size and a controlled and well-developed mesoporous structure[11,12,10].

In literature it is possible to notice an increasing interest for zirconium(IV) oxide nanoparticles. Firstly, in the case of environmental remediation, for the affinity between zirconium(IV) oxide and phosphates, that could be a solution for eutrophication of water. Phosphorous is an essential element, widely used both in agriculture and industry, but an excess can cause a severe pollution of water. Conventional phosphorus removal methods from wastewater include chemical precipitation, biological processes, reverse osmosis and also sorption processes. Adsorption is a promising method to treat water pollution, especially at lower phosphate concentrations. So in the last decades many studies have been focused on materials selection that have a good performance for P adsorption. Among all, hydrous zirconium oxide has remarkable selectivity

to phosphoric ion and also high resistance to acids, alkalis, oxidants, and reductants. Fe-Zr binary oxide nanoparticles are mentioned by several authors, because of their good adsorption of pollutants, such as arsenic[13] and phosphate. A probable mechanism involved in this process concerns the formation of inner-sphere surface complexes of phosphate anions at the water/oxide interface[14,13,15]. Mesoporous zirconium oxide nanoparticles have a good performance in removal of phosphates from wastewaters, too, because of a physicochemical attraction and ion exchange process[16].

This great selectivity of zirconium can be used in biology for detection of protein phosphorylation, which plays a critical regulatory role in many vital biological processes such as cellular signal communications during development, physiological responses, homeostasis, neural activities, immune response, etc[17]. It can be also used as protein or DNA probe in microarrays. In fact, recent technologies need selective methods for surface immobilization and innovative strategies compared to antibodies as capture agents both in DNA and proteinmicroarrays[18]. This material could also be useful for detection of some marker protein of cancer or other diseases[19].

Zirconium(IV) oxide nanoparticles find their place also in nanomedicine. For example, the antimicrobial activities of zirconium(IV) oxide (ZrO_2) nanoparticles and other complexes of zirconium and various ligands were studied on several bacterial or fungal strains[20,21]. In a case study, nanoparticles of 50 nm of diameter have been used. It was assessed that antimicrobial activity depends on the size and the shape of the nanomaterial[22]. Besides all these applications, zirconium(IV) oxide nanoparticles are mentioned for drug delivery, too. Some examples are the synthesis of mesoporous titanium zirconium oxide nanospheres as drug carrier for bone-related complications[23] or hollow mesoporous zirconium(IV) oxide nanocapsules, used as vehicles for anti-cancer drug delivery[24] or mesoporous zirconium(IV) oxide nanospheres loaded with anti-cancer drugs[10].

Because of these opportunities, studies on the morphological control and surface functionalization of zirconium(IV) oxide nanoparticles open new platforms for various biotechnological and biomedical applications, like mesoporous silica nanoparticles, the most used inorganic system reported in the literature. There is great interest to synthesize this new system, with large surface areas, tailorable pore sizes, controlled size and shape and functional surfaces in order to verify new horizons and to test them in a variety of applications such as the bone reconstruction.

1.4 Hydroxyapatite nanoparticles

Hydroxyapatite is one of the most used biomaterials whose main applications are replacing and coating bone implants. Natural bone is made up of collagen fiber matrix stiffened by hydroxyapatite crystals that account for 69% of the weight of the bone. So HAp-polymer composites are often fabricated to mimic biological processes or to facilitate bone repair, being osteoconductive, with both synthetic and biological macromolecules. This high biocompatibility does not cause an inflammatory or toxic response beyond an acceptable tolerable threshold. Moreover, a biomaterial for bone implants must have appropriate mechanical properties, closest to what it replaces. Synthetic HAp is used because it is bioactive and it arouses a direct chemical response at the interface and forms a very tight bond to tissue. The main drawback of this material is its poor mechanical properties, such as low strength and limited fatigue resistance. To overcome these shortcomings composites are fabricated. For example, HAp is inserted in different weight % ratio into zirconium or titanium to enhance its mechanical properties. Common uses include bone graft substitution and coatings on metallic implants.
It can be synthesized by a variety of methods, such as co-precipitation or sol-gel. Hydrothermal synthesis allows to have needle-like particles with dimensions ranging between 20 - 40 nm in diameter and 100 - 160 nm in length. Its properties can be influenced by controlling its size, but also its chemical composition and morphology. Template synthesis can be convenient to regulate the nucleation and crystal growth. Temperature and reaction times are also critical parameters to take into account. Furthermore, a preferred orientation is believed to affect its performance to control the cellular behaviour and to enhance the tissue mineralization[25,26,27,28].
There are also rising interests in bone scaffolds or cements which are not only biosafe or osteoinductive, but also antimicrobial. In fact, infections are a big problem in all kind of surgery, especially in orthopaedic one[29].

1.5 Nosocomial infections

Nosocomial infections can be defined as those occurring during hospital admission. They affect 1 in 10 patients. Immunodeficient patients and babies are the first victims of these infectious diseases. Annually, these result in 5000 deaths. One of the most common causes of these infections is *Staphylococcus aureus.* The major problem of this pathogen is its great ability to develop resistance to antibiotic therapies. Generally, bacteria become resistant when they acquire new genetic material, which can be then transferred to other strains. Methicillin-

resistant/susceptible *S. aureus* causes up to 60% of nosocomial infections. This includes also all the infections to medical devices, as prosthesis, heart valves, catheters, etc. Vancomycin is usually prescribed in these cases, because it's a broad-spectrum antibiotic. So, the knowledge of emerging pathogens and resistance profile is essential for treatment against these infections. In fact, a shorter and more appropriate therapy is recommended to reduce the selection for resistant isolates[30,31].

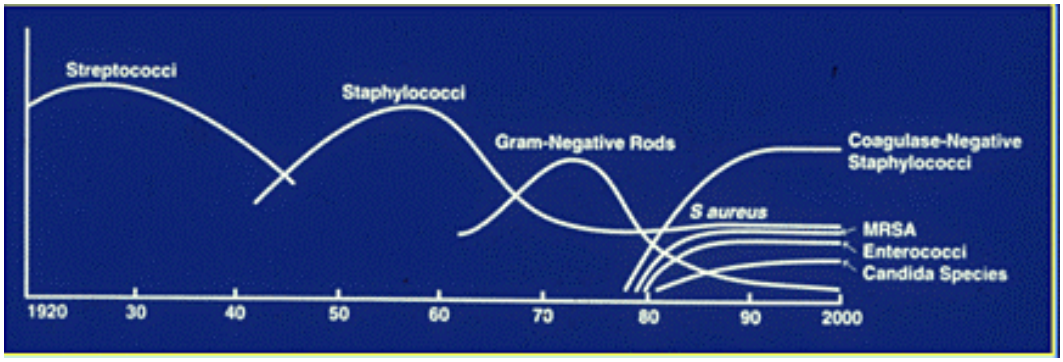

Figure 1.5 Major nosocomial pathogens of the 20th century. Streptococci and Staphylococci are the major players of these infections (R.A. Weinstein, MD).

1.5.1 Staphylococcus aureus and Gram-positive bacteria

Staphylococcus aureus is a Gram-positive coccus with a diameter of 0.5 to 1.5 µm, whose colonies are recognizable as circular and yellowish in culture. Gram-positive refers to bacterial strains that are positive to Gram stain, because of the differences between cell walls in Gram-positive and negative bacteria.

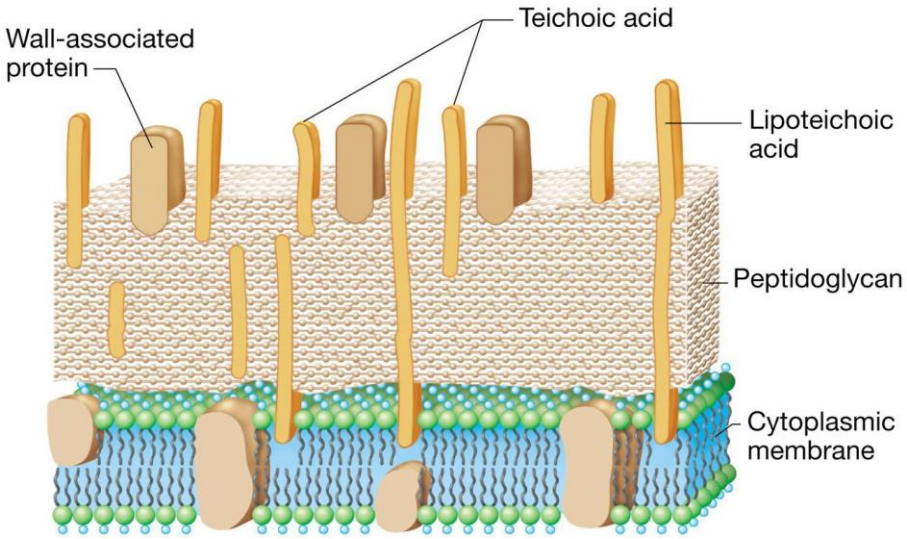

Figure 1.6 Gram-positive cell wall and cytoplasmic membrane. The peptidoglycan represents the main component in Gram-positive bacteria cell wall. Teichoic/lipoteichoic acids are inserted into the cell wall and confers a negative charge to the cell wall of these bacteria (Madigan et al. 2012)[32]

Despite of Gram-negative, Gram-positive bacteria have a thick cell wall, primarily made up of a polysaccharide, the peptidoglycan. The last one consists of the repetition of an unit, called glycan tetrapeptide, formed by N-acetylglucosamine and N-acetylmuramic acid, and three to five amino acids (which can be also D-aminoacids).

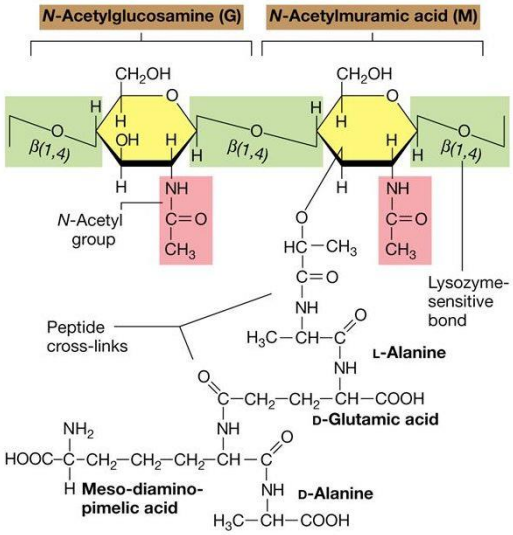

Figure 1.7 Unit of repetition of peptidoglycan (Madigan et al. 2012)[32]

These chains of peptidoglycan are linked by amino acid bridges. Gram-positive bacteria cell wall contains also teichoic acids. These are polyalcohols covalently linked by phosphate esters and sugar or amino acids, such as D-alanine.

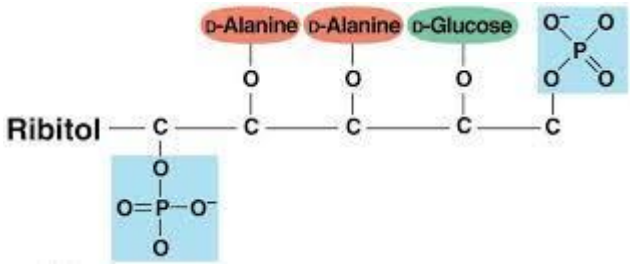

Figure 1.8 Teichoic acid of Gram-positive bacteria, polymer of ribitol (Madigan et al. 2012)[32]

The cell wall is very important for bacteria. It has many functions, and it is used as osmotic, chemical and mechanical protection, in addition to giving a shape to the cell itself, and to allow transport, anchorage, metabolic, immune and virulence functions[32].

Staphylococcus aureus is responsible for the majority of superficial and invasive skin infections[33], endocarditis, osteoarticular infections, as osteomyelitis, septic arthritis, prosthetic devices infection, pleuropulmonary and urinary tract infections, meningitis, and other serious diseases. Most of them are caused by biofilms, starting from asymptomatically colonization of the host[34,35,36].

The major problem found in fight this bacterium is its great ability to become resistant to antibiotics. In fact, the emergence of antibiotic resistance by *S. aureus* can be visualized as a series of waves. The first one began in 1940s with the infections of penicillin-resistant *S. aureus* that in 1950s became pandemic. This infection disappeared with the introduction of methicillin, indeed, between 1957 and 1973 methicillin-susceptible *S. aureus* (MSSA) strains were isolated. In 1960s a report of the first methicillin resistant strain of this pathogen (MRSA) was published. The gene responsible of this resistance, *mecA*, was only discovered 20 years later. The increasing burden of MRSA infections, especially in hospitals, led to the usage of vancomycin and these infections continue to the present time. In last few years, some strains were found as vancomycin-intermediate *S. aureus* (not inhibited at VCN concentrations below 4 to 8 µg/ml) and vancomycin-resistant *S. aureus* (not inhibited at VCN concentrations below 16 µg/ml)[35].

1.5.2 Vancomycin

Vancomycin is a glycopeptidic antibiotic, produced by *Streptomyces orientalis*. It is known to be effective especially against MRSA, but also against MSSA. It is generally used when all other treatments have failed.

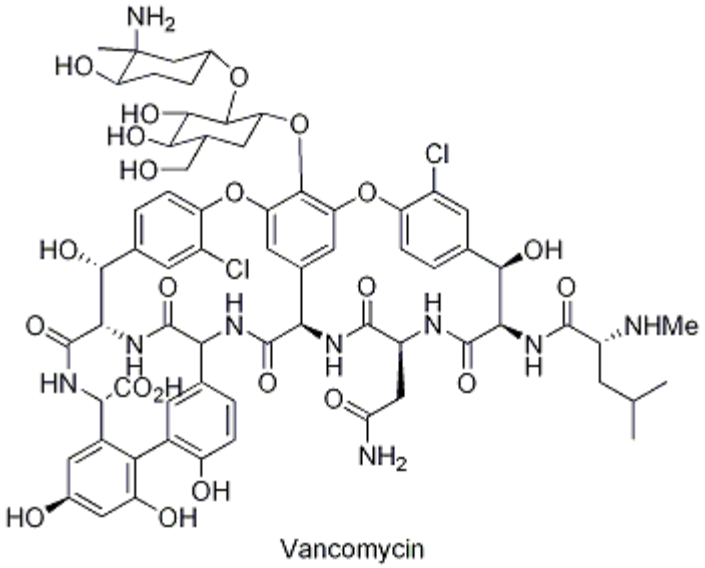

Figure 1.9 Vancomycin glycopeptide structure

This antimicrobial agent inhibits the biosynthesis of peptidoglycan. This mechanism of action is related to the ability of VCN to bind to D-alanyl-D-alanyl moieties (via hydrogen bonds), that are present in various phases of the polymer synthesis. In fact, it prevents the enzyme transpeptidase from acting in the reformation of the peptide cross links (transpeptidation). So, through steric hindrance, VCN makes the peptidoglycan layer less rigid and more permeable, due to its ability to prevent the cross-linking of these layers[37,38]. The spectrum of activity of this antibiotic consists of: *Staphylococcus aureus;* Coagulase negative *Staphylococci; Streptococcus pneumonia; Streptococcus spp; Enterococcus spp; Clostridrium spp.; Actynomyces.* These are all Gram-positive bacteria: VCN is ineffective against Gram-negative bacteria because its high molecular weight (1449.3 g/mol) prevents it to pass through the outer membrane[39]. The VCN resistance regards the replacement of D-Ala-D-Ala with D-Ala-D-lactate residues, reducing the binding of the antibiotic to its target[40].

Vancomycin is primarily administrated orally or intravenously, but as any drugs it could cause toxic reactions. There are a lot of reports regarding the ototoxicity and nephrotoxicity of the antibiotic, especially in the first years of its use. This toxicity clearly depends on its aggressive dosing and especially depends on patients' sensitivity[41,42]. To overcome these problems, nanotechnologies aim to have a controlled and site-specific release. In literature, there are a lot of works dealing about this aspect. The main expected application regards the orthopaedic surgery, since VCN is used in perioperative antibiotic prophylaxis. Principal targets in this case were *S. aureus* or *S. epidermidis* infections and especially the biofilm formation on prosthetic devices. For example, silica nanoparticles or matrices are often used. Kurczewska et al. (2015) described a vancomycin-modified silica matrix. The chemical bonding affects both drug release

and biological activity. They observed that weak bonding gives rapid release, compared to the uniform rate of the VCN release of covalently bonded substance or to the very weak drug release in case of strong ionic bonding, which is anyway inefficient from a therapeutical point of view. This modulability is very important for practical applications, as tissue rigeneration[43]. VCN-loaded mesoporous silica nanoparticles are also mentioned in composites with calcium sulphate, for artificial bone or bone cement. Gu et al. (2016) evaluated the biocompatibility of an artificial bone based on these composites for treatment of bone defects, as fractures[44]. Similarly, Li et al. (2015) described these composites as bone cement with a prolonged and local release[45]. Silica is just an example of biomaterial used in these cases. Indeed, calcium phosphate[46] bone cements, hydroxyapatite coatings on titanium implants[47] or hydroxyapatite nanocomposites with collagen[48] or other biocompatible polymers[49], injectable gellan gum-based nanoparticles[50] and other DDSs[51,52] were loaded with VCN and reported in literature as promising biomaterials with also antibacterial properties. This shows the great interest for medicine to use VCN also in these new experimental treatments.

In the case of a biofilm formation, the major problem is the inefficacy of the antibiotics, included vancomycin. In fact, except for high concentrations of drugs, antibiotics don't inhibit their formation or don't cross the biofilm barriers[53,54]. Nanotechnology could overcome this limit.

1.6 Biofilms

A biofilm is a sessile community characterized by bacteria or fungi that are attached to a substratum or interface or to each other. These cells are embedded in a matrix of extracellular polymeric substances that they have produced and they can colonize both abiotic and biotic surfaces[55].

1.6.1 Biofilm formation

Biofilm formation is a complex dynamic process. Firstly, bacteria adhere to the surfaces in a reversible association, then through irreversible attachment, and finally develop into an adherent biofilm of highly structured and cooperative consortia. Mature biofilms typically consist of differentiated mushroom- and pillar-like structures of cells embedded in extracellular polymer

matrix. In the biofilm structure, there are water-filled channels and voids through which nutrients, oxygen, and metabolic wastes can flow. The adherence to surfaces is dictated by different variables, including the species of bacteria, surface composition and nature, nutrient and water availability, cell-to-cell communication. It's known that bacterial cells communicate through the secretion and uptake of small diffusible molecules. This process is called quorum sensing (QS, see paragraph **1.6.1.1**) [36].

Different processes take place during the interaction between bacteria and the surface. On an abiotic surface, the primary attachment is generally mediated by non-specific interactions such as electrostatic, hydrophobic, or van der Waals forces, whereas adhesion to biotic surface, such as biological tissues, is mediated by specific bonds (lectin or adhesin). The bacterial adhesion is affected by surface hydrophobicity, which is determined by bacterial surface-associated proteins. Motility is another very important factor for the planktonic cells to make initial contacts with an abiotic surface and it can play a role in their pathogenesis. After binding to the surface through exopolymeric matrix, the irreversible adhesion can start. These extracellular matrices consists of a mixture of materials such as polysaccharides, proteins, nucleic acids, and other substances, essential for the biofilm structure, for biofilm growth and for the protection of cells from dehydration and other biotic or abiotic stresses such as antimicrobial activity. High molecular weight exopolysaccharide polymers, possibly microbial DNA, and surface proteins are used to efficiently retain the bacterial cells within the biofilm matrix. Many genes with related function are regulated at the transcriptional level, permitting microorganisms to switch from planktonic to sessile forms under different environmental conditions[36].

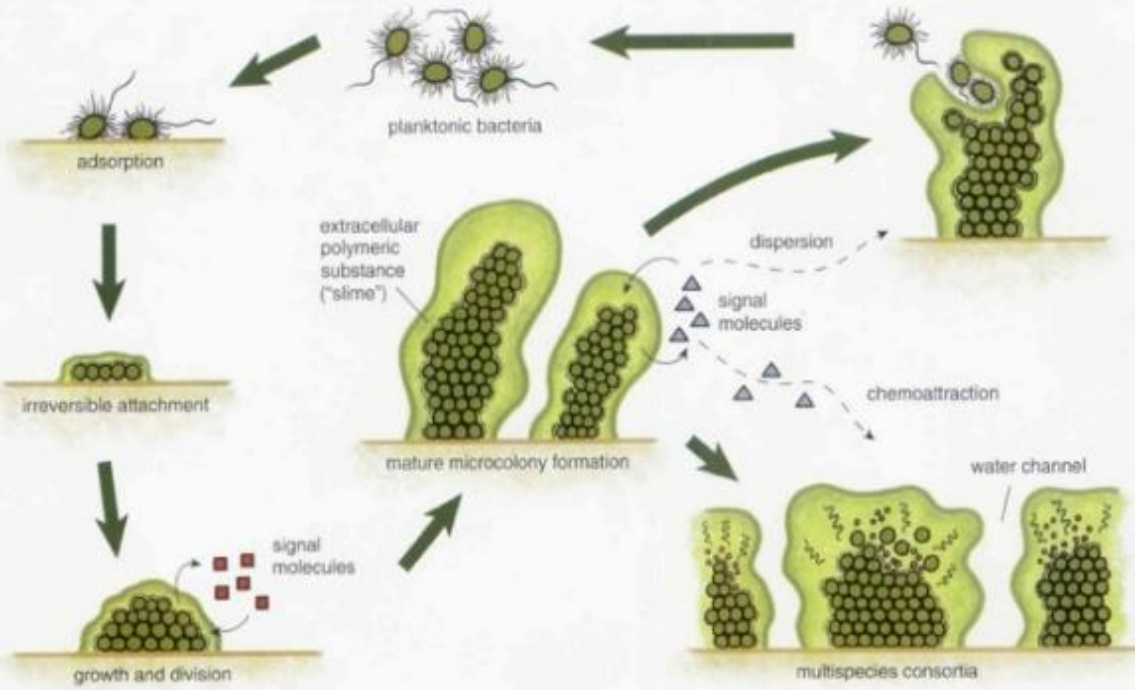

Figure 1.10 Different steps of biofilm formation process in different steps. Main phases of biofilm formation consist of adhesion to an abiotic/biotic surface. Bacteria release exopolysaccharides matrix and, communicating with signal molecules, the irreversible adhesion can take place. Finally, they can organize a mature structure, with water channels, also including multispecies consortia. Bacterial biofilm can release planktonic cells to colonize other surfaces. (Olson et al., Canadian Journal of Veterinary Research, 2002)

Bacterial cells detached from the biofilm re-enter the planktonic state, in order to colonize new virgin areas. Indeed, biofilm formation in considered cyclical. Nutrient starvation, overexpression of some proteins, probably QS-mediated, and loss of EPS, are involved during biofilm detachment[36].

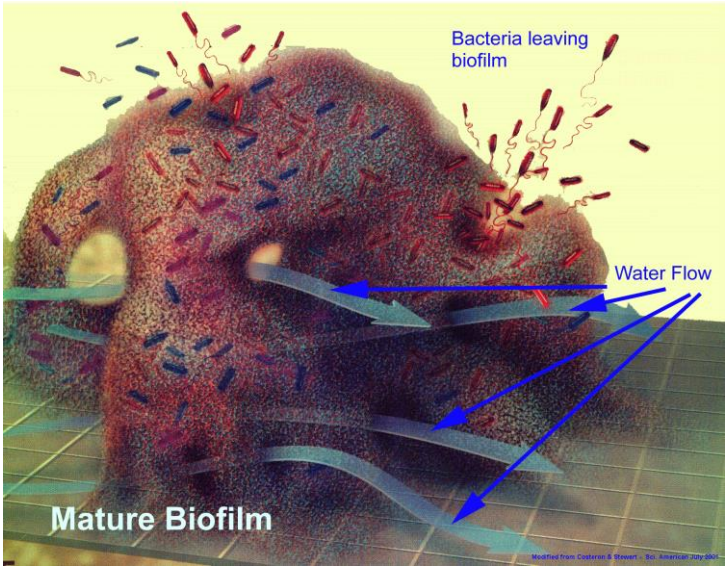

Figure 1.11 Mature biofilm structure where water flow channels and the release of planktonic bacteria are visible. (American society for Microbiology)

1.6.1.1 Quorum sensing

Quorum sensing is a mechanism of cell-to-cell signalling, regulated by gene expression, that starts at a certain level of population density. In this way bacteria can coordinate their gene expression, modifying their motility, virulence, sporulation, development of structures as biofilm etc., just sensing the environmental changes. Indeed, dozens of bacterial signals have been discovered. These span from amino acids to short cyclic signal peptides in gram-positive bacteria. These signal molecules are dispersed in the surrounding environment and transported to bacterial cells through their membrane or active mechanisms. Since QS mechanism requires high cell density, in the early stages of biofilm formation these molecules may not be produced; however, they can play an important role on mature biofilm differentiation. QS is dependent on the diffusion path between planktonic cells[36].

1.6.2 Biofilm resistance

The resistance of biofilm bacteria to antibiotics is considered a general phenomenon. Usually biofilms are more resistant than planktonic bacteria. When bacteria are exposed to antimicrobial agents, a small part population of persistent bacteria can survive and repopulate the surface immediately, becoming more resistant to the antimicrobial treatment. In contradiction, if dispersed from the biofilm, those bacterial cells can revert to an antimicrobial agent susceptible

form. A lot of theories try to explain biofilm resistance to drugs. About the antimicrobial agents failure to penetrate the biofilm EPS, some authors hypothesize a possible neutralizing reaction by biofilm. Other researchers identify quorum sensing as a key mechanism to up-regulate the resistance. It could also depends on the physiology of bacterial strain[56]. Other additional factors are involved for the resistance of biofilm cells, including the presence of a diffusion barrier that can affect the path of the antibiotic, the possible interaction of exopolymer with the antimicrobial agents, hypermutation and possible presence of certain resistance genes. Bacterial extracellular matrix can improve their resistance to the antimicrobial molecules and, in case of biotic surfaces, to the cells mobilized by the host.

The increasing use of medical implants or devices has increased the incidence of these infections which invariably involve biofilms of some microorganisms, such as *S. aureus*, intrinsically resistant to multiple antibiotics. The chronic nature of biofilm infections increases this problem. Due to their painless nature, biofilm-related infections are usually diagnosed when they have already been established. This makes biofilm eradication more attractive than biofilm inhibition. Solutions to this problem generally involve the replacing of the infected medical implant. To overcome such an invasive operation, it would be useful using biomaterial resistant to bacterial colonization or able to incorporate antibiotics[36].

1.6.3 Medical device- related and nosocomial infections

Medical device-related infection is a problem for patients who benefit from temporarily inserted or long-term implanted devices. The biofilm mode of growth on medical device biomaterials is important because it can confer some advantages on bacteria, as resistance to antimicrobial agents. However, it can cause serious detriments to patients. Catheters, prosthesis, contact lenses, hip joints, cardiac valves, intraocular lenses and other medical devices are subjects to microbial biofilm formation. The problem arises for implants that need complex surgeries to treat the infection, removing the system. This can be crucial for resistance mechanisms. The development of used biomaterials, or surface coatings and treatments, drug-incorporated bulk polymers and coatings, the availability of novel biodegradable polymers and also nanotechnologies can find a way to overcome this trouble. Furthermore, the contact between medical devices and biological fluids can be a determining factor in the adherence and colonization of a microbial pathogen and this depends on the composition of the eventual secretion. The formation of a conditioning film is a very important event because it alters the surface of the biomaterial and may provide sites for bacterial adhesion. As the process of microbial adhesion is the initial event in the pathogenesis of infection, the prevention of this

stage results in removal of the microorganism from the surface of an implants, avoiding eventual surgeries. The adherence of a microorganism to a medical device surface consists of different levels of complexity and is influenced by a number of parameters such as the bacterial cell wall characteristics, the nature of the fluid interface, and the biomaterial composition and characteristics.

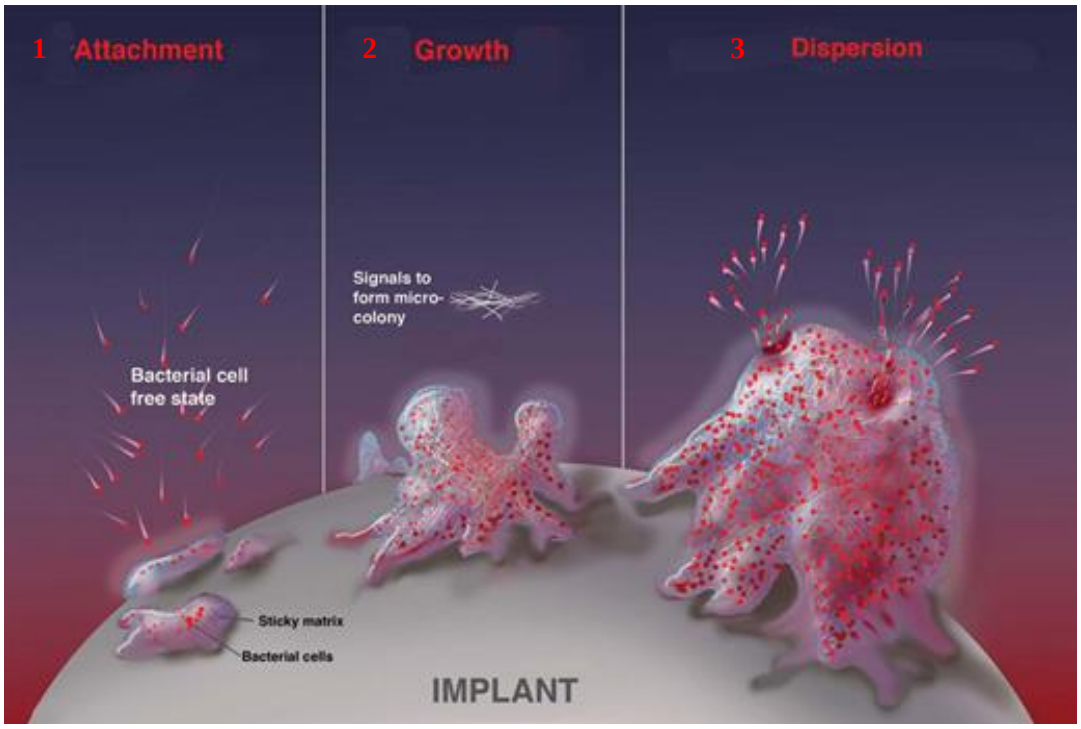

Figure 1.12 Biofilm infection on an implant consists of three main steps: 1) adhesion to a surface, 2) biofilm growth, using communication with signal molecules and 3) dispersion of planktonic cells (Wixtrom et al. 2012)[57]

The first organisms attaching are the primary colonizers: if the conditions are suitable, they can then multiply. Sometimes, a process called coadhesion occurs: other bacterial cells from the planktonic population specifically adhere to cells in the biofilm and may provide for a multispecies biofilm community. The different stages involved into medical-devices infections were studied by analyzing the interaction between bacterial and biomaterial surfaces. These stages consist of more or less random microbial transport to the surface, followed by an initial adhesion which can be temporary or irreversible. Under suitable conditions this process results into the attachment to medical-device surface and colonization with a mature biofilm[36].

The use of prosthetic devices has certainly impacted patients' quality of life, improving their life and giving them their independence. Orthopaedic device infections are however one of the most devastating complications in this case, because they often imply subsequent surgeries, prolonged antimicrobial therapies, amputation in some instances, and occasionally morbidity and death. So, in recent years, researchers are developing systems with both antimicrobial and regenerative activities. A possible target of these studies could be also MSCs (mesenchymal

stem cells), that are considered a new diagnostic tool, as "biomarkers" for a non-invasive diagnosis[36,58].

1.6.4 *S. aureus* biofilm

The Gram-positive bacterium *Staphylococcus aureus* is an ubiquitous pathogen. It can be harmful to humans and its colonization predisposes to infection. *S. aureus* can invade, colonize, producing a disease when surgeon trauma, medical procedures, devices implantation, or injections disrupt the skin or mucous membrane barrier. The diseases most commonly associated with *S. aureus* are skin, soft tissue, bone and more in general, nosocomial infections. Indeed, *S. aureus* infections are very invasive and include nosocomial pneumonia, bacteremias, and endovascular infections like endocarditis and septic thrombophlebitis, which can cause embolism. *S. aureus* is also a frequent cause of medical device and implant-related infections, linked to an increased incidence in nosocomial *S. aureus* bacteremias. *S. aureus* infections are difficult to treat, often needing weeks of intravenous antimicrobial therapy. Severe infections that involve implants require surgical removal of the implant for successful cure. If not treated aggressively, the infections can recur and develop into chronic problems. *S. aureus* related infections have a significant negative impact on patient outcomes and overall costs. Even if in the last few years *Staphylococcus epidermidis* was considered the prototypical Gram-positive biofilm organism, especially related to implant infections, *S. aureus* biofilms were found on intravascular catheters, explanted pacemaker leads, within bone and on heart valves. Moreover, *S. aureus* can produce the same slime as *S. epidermidis*[36].

Biofilm pathogenesis consists of a three-step process and is similar to the process already described in paragraph **1.6.1**. The initial stage of biofilm pathogenesis is the adhesion of microorganisms to a biological or inorganic surface. The second stage involves cell proliferation on the surface and the production of an exopolysaccharide matrix to facilitate cells aggregation. The third stage is the organization of bacteria into three-dimensional structures with channels through which nutrients and waste products can flow. In the biofilm, bacteria seem an integrated community. *S. aureus* in the early stages of attachment to surfaces shows differences in physiology between adherent and planktonic cells. Adherent bacteria have slower growth and decreased metabolism than planktonic ones. Resistances to the cell wall active β-lactam and glycopeptide antimicrobials can be attributed to the decreased growth rate of the adherent bacteria and this proves the existence of both planktonic and biofilm forms. Two main aspects of the biofilm are relevant to clinical disease: the antimicrobial resistance (minimal biocidal

concentration is 2 to 1,000-fold higher than planktonic one) and the inability of the host immune cells, as leukocytes, to kill the biofilm bacteria. So, the antimicrobial therapies frequently fail. In respect of the differences between two phenotypes, five genes are upregulated during biofilm growth. In particular, three of these genes encode for an enzyme of the glycolysis or fermentation pathway and other two genes encode for an enzyme that may help *S. aureus* adapt to nutrient limitation[36].

The approach to treat *S. aureus* biofilm infections consists of antimicrobial therapy and proper surgical resection and debridement. However, the emergence of new resistant *S. aureus* strains is a reason to find alternative approaches, among them the surface modification of implants with antimicrobial agents. Disruption of global gene regulator circuits also offers a new target to affect the expression of biofilm determinants and possibly improve the efficacy of standard therapy[36].

1.6.5 *In vitro* and *in vivo* biofilm studies

The study of biofilm to test antimicrobial agents and new therapies is of increasing interest in the last decades. A number of methods for biofilm growth evaluation are available. An important parameter used to evaluate an antibiotic efficacy is the minimal inhibitory concentration (MIC), namely the minimal concentration needed to prevent the bacterial growth. However this value is calculated on planktonic cells: usually biofilms show a good resistance against antibiotic treatment, even at concentration higher than MIC. Furthermore, some antibiotics have different *in vitro* and *in vivo* MIC values . Resolution of this problem could be achieved by utilizing an assay system that can select antibiotics and biocides based on activity against biofilms. The MBEC represents the concentration of antibiotic or biocide capable of eradicate a biofilm and would be the equivalent to the MBC that determines the inhibition of the biofilm growth. The aims of recent studies are selecting for new antimicrobial agents that are effective against biofilms, selecting more suitable antimicrobials for every patient therapy, and overcoming the problem of drug resistance related to the biofilms.

The criteria for a successful biofilm assay will include the ability to form biofilms of different organisms, and to learn much more about their formation mechanism, separating adherent from planktonic bacteria. Indeed, there has been an explosion of interest in biofilms, biofilm morphology and biofilm physiology, but also in all the possible therapies against them *in vitro* and *in vivo*[36]. The most commonly employed culturing methodologies, also suitable to mimic *in vitro* what happens during the biofilm infections (for example the adherence on an abiotic

surface) are static microtiter plate assays, flow cells, tube biofilms, colony biofilms, rotating disk and concentric cylinder reactors, biofilm growth on PEG lids.

Static microtiter plate assay was developed to quantify the extent of an infection on an abiotic surface and has the advantages of relatively high-throughput screening and to evaluate the effects of environmental parameters on the ability of bacteria to colonize and form biofilms. Flow cells system consists of a chamber where biofilm bacteria are grown, usually attached to a coverslip and with the introduction of various fluorescent proteins and dyes, it enables the analysis of the spatial distribution and growth of individual cells in real time. Furthermore, it can be used in conjunction with fluorescent reporter genes to study spatial patterns of gene expression and it is suitable to examine biofilm formation on biological surfaces. Tube biofilms system consists of a platform for studying biofilms that develop under flow., Biofilms are grown on the interior surface of silicone tubing, enabling the accumulation of a large biofilm mass, useful to test antimicrobial agents. Colony biofilms are grown on a semi-permeable polycarbonate filter placed onto an appropriate solid medium; this test is useful to develop biofilm at the air–surface interface. Rotating disk and concentric cylinder reactors are developed to grow biofilms under shear stress for the reproducible evaluation of biocide efficacy[59]. Biofilm growth on PEG lids overcomes the problems of other high-throughput methods and possible contamination. An example of this technique is the Calgary biofilm device, which consists of a polystyrene lid with 96 PEGs into a standard 96-well microtiter plate (Fig. **1.13**)[59,60].

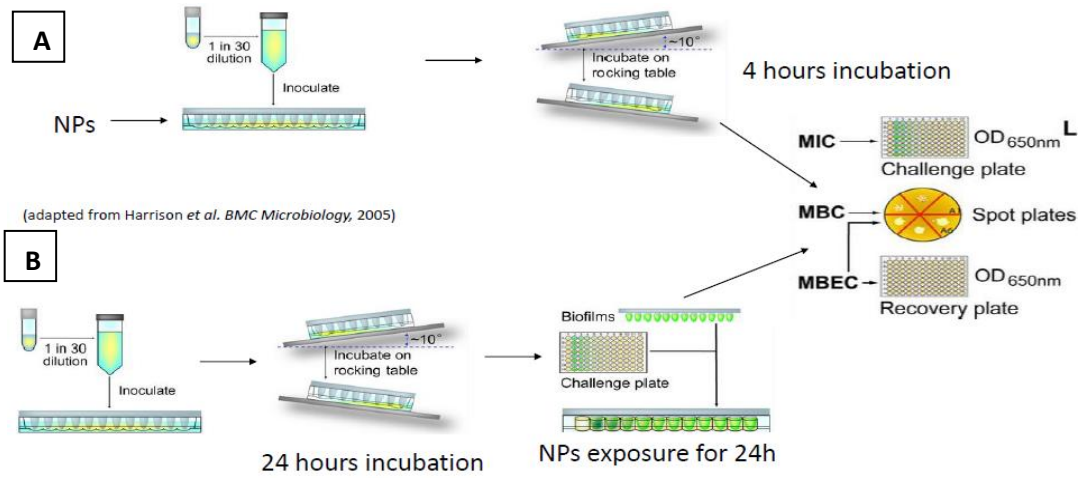

Figure 1.13 Calgary device for biofilm inhibition/eradication studies, adapted from Harrison et al. 2006. This is an high throughput screening device useful to evaluate the capability of the antimicrobial agents to prevent the formation of biofilm or to eradicate a preformed biofilm on the PEG lids. **A)** inhibition test procedure: the inoculum of the bacterial strain is directly made into the medium containing the agent to be tested. **B)** eradication test procedure: after the inoculum, biofilm is left to grow on the PEG lids; medium is then changed with another containing the antimicrobial agent[60].

Therefore, a variety of *in vivo* models have been developed to study biofilm and especially antibiofouling therapies. Anyway, many factors must be considered in the development of an animal model suitable for the study of biofilm-associated infection. The organism's ability to adhere to the biomaterial, colonize it and develop biofilm should be verified before beginning any *in vivo* studies. The development of new models will hopefully result in increased reliability while granting reproducible data to treat biofilm associated infections[36].

Another type of valuable analyses on biofilms is microscopy. The major example is the confocal laser scanning microscope (CLSM) which allows to magnify live cell in real time. This is a non-invasive and non-destructive technique which consents to obtain a 3D imaging and it is useful to gain information about biofilm behaviour and quantification[61].

1.6.6 Nanotechnology and biofilms

The increasing interest to antibiofouling therapies opened a way to nanotechnologies, knowing about the biofilm resistance to conventional antimicrobial agents. Furthermore, nanoparticles allow to avoid toxic effects of the drug with controlled and local release. Examples of these applications are both inorganic and organic nanoparticles. An example of inorganic ones is that described by Zonaro et al. (2015)[60]. In this case, selenium and tellurium nanoparticles were used against both planktonic and biofilm forms of three common pathogens, analysing the toxic effect produced by ROS at increasing concentrations of nanoparticles[62]. Gold-nanoparticles were also tested against biofilm, but in complexes with antibiotics, to increase their activity[63]. Some works describe the coating of biomedical devices surface with nanoparticles that show antibacterial activity as Ag NPs or MgF_2[64]. The most common used DDSs used against biofilm are organic nanostructures as liposomes or polymer-based systems especially because of their biocompatibility, such as chitosan nanoconiugated with VCN[65,66,67]. In general, nanostructures can act against biofilm producing ROS, closing the nutrient and oxygen channels interspersed into biofilm structure or conveying the drug through the exopolysaccharides barrier. For all these reasons and because of their scalability and the possibility of opportunely functionalize them, nanotechnologies have a promising future in this biomedical field.

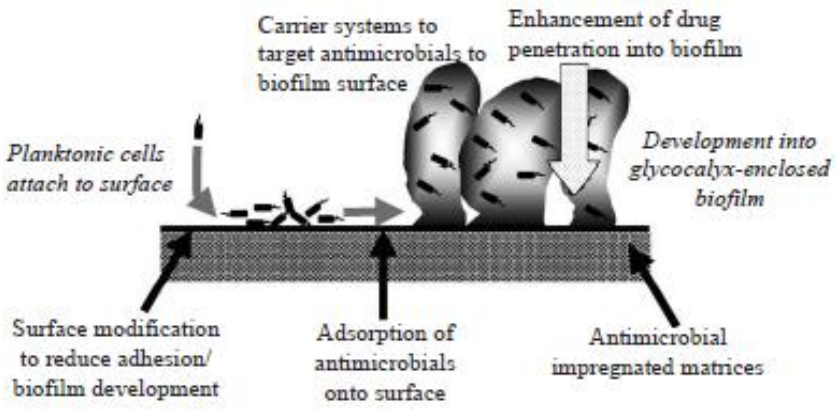

Figure 1.14 Main anti-biofilm strategies (Smith, 2005)

2 Aim of the work

This work aims to show two of the main aspects of nanomedicine: drug delivery and regenerative medicine.

MZNs were synthesized and loaded with VCN, a glycopeptide used against Gram+ bacteria. This antibiotic molecule interferes with the synthesis of the peptidoglycan of bacterial cell wall and it is commonly administrated as antibiotic prophylaxis in orthopedic surgery. In fact, one of the most serious problems in medicine is the risk of contracting the so-called nosocomial infections, often caused by *Staphylococcus aureus*, that generally forms biofilm on biomedical devices. With this work, VCN-loaded NPs were tested in order to assess their activity against planktonic and biofilm bacterial cells of *S. aureus*. Results were compared with the free form of the antibiotic.

On the other side, knowing from literature about the affinity of zirconia and phosphates, MZNs were coated with a shell of HAp and bis-phophonate, to test them in cell cultures of MSCs and evaluate both their biocompatibility and a possible role in the osteogenic differentiation.

3 Summary of the work

MZNs were synthesized, characterized and loaded with VCN in different conditions. The release of the drug was carried out under the same conditions of the loading. Antibacterial tests in liquid and solid media were conducted against *S. aureus* ATCC 6538 and results were compared with free drug activity. Antibiofouling experiments were performed using Calgary device. Activity of VCN-loaded NPs were compared with the free drug against *S. aureus* biofilm. Both eradication and inhibition tests were conducted. Biofilm of *S. aureus* were grown in static conditions on glass cover slips, to test both MZNs and VCN-loaded MZNs.

MZNs were coated with a shell of hydroxyapatite, synthesized by hydrothermal treatment. These NPs were characterized and loaded with VCN. Release and preliminary antibacterial and antibiofouling tests were conducted with VCN-loaded HAp-MZNs.

Both MZNs and HAp-MZNs were further functionalized with a bis-phosphonate and marked with R6G, to perform biocompatibility and osteogenic differentiation tests on MSCs.

4 Experimental section

4.1 Materials

All reagents were ACS grade and were all used as received. APTES, Na_2HPO_4, NaH_2PO_4, R6G, K_3PO_4,$CaCl_2$, $Na_3C_6H_5O_7$, Trizma® base, CH_2O, toluidine blue, bacteriological Agar for molecular biology, dialysis tubing cellulose membrane (MWCO: 14kDa) were purchased fromSigma-Aldrich. Absolute EtOH from AnalaR Normapur; NaF, HCl (37%), NaCl, $Zr(OPr)_4$ solution, HDMS and monohydrate D-(+)-glucose for microbiology from Fluka. 1-hexadecylamine from Alfa Aesar; CAPS acid from USB; glacial acetic acid from Chimica Milano. VCN of Vancotex (500 mg) used for loading experiments and DAPI for CLSM images were kindly provided by IOR of Bologna; TSB and MSA from Biolife, gently provided by ARIES s.r.l.; nutrient broth and nutrient agar from OXOID, kindly given by PhD Zonaro and prof. Lampis of University of Verona; bis-phosphonate: 2-phenyletene-1,1-diyldiphosphonic acid was synthesized and gently given by prof. Alessandro Scarso's group. For all aqueous solutions MilliQ water was used.

4.2 Characterization

Dimensions, morphologies and sample composition were assessed using a FE-SEM (Field Emission Gun - Scanning Electron Microscope), Σigma from Zeiss. Mean nanoparticles diameters were calculated measuring at least 100 nanoparticles, using the image analysis software ImageJ. DLS and ZP measures were conducted at the University of Verona using Zetasizernano SZ3600 equipped with a laser at 633 nm and at VEGA with NICOMP 380 ZLS. The nitrogen adsorption-desorption isotherms were measured at liquid nitrogen temperature, -196°C, using a Micrometric ASAP 2010 volumetric adsorption analyzer. The specific surface area was calculated from BET equation and the pore size distributions from BJH. UV-vis measurements for drug loading, drug release, and bacterial growth were recorded on UV-Vis spectrophotometer Agilent 8453 and Nanophotometer Implen. TGA and DSC were performed using a Linseis STA PT-1000 under nitrogen flow from 30°C to 900°C with heating rate of 20°C min^{-1}, to compare drug loading measures obtained from UV-Vis spectrophotometer. The emission of R6G-loaded NPs was determined using a spectrofluorometer Perkin Elmer Victor 3V 1420 multilabel counter. A Philips X'Pert vertical goniometer with Bragg Brentano geometry, connected to a highly stabilized generator, was used for XRPD measurements. A focusing graphite monochromator and a proportional counter with a pulse-height discriminator were used. Nickel-filtered Cu kα radiation and a step-by-step technique were employed with steps of 0,05° for 10 s from 5 to 140° and steps of 0,02° for 30 s from 32 to 35°. All photos for antibacterial tests on agar were taken from a Perkin Elmer Geliance 600 Imaging System. The IR spectra were recorded using Nexus FT-IR instrument implementing a Nicolet AVATAR Diffuse Reflectance accessory. TEM micrographs and electron diffraction pattern were collected by JEM 3010 (JEOL) electron microscope at 300 kV of accelerating voltage. Sputter coater Polaron SC7620 was used to prepare the glass coverslips with biofilm for SEM analysis.

Thanks to IOR of Bologna for CLSM images and BSc, PhD Maria Teresa Valenti for MSC tests.

4.3 Methods

4.3.1 Synthesis of mesoporous zirconia nanoparticles

In a flask of 250 ml 0,908g of hexadecylamine were dissolved in 90,26 ml of ethanol under vigorous stirring at room temperature. 0,622 ml of MilliQ water and 0,366 ml of NaF 0,1 M were then added to this solution. In a vial 0,909 ml of the precursor, $Zr(OPr)_4$, was mixed with 1,143 ml of EtOH, under stirring for 15 minutes, until the two phases disappear and the solution became clear and yellow. This second solution was added dropwise into the first solution under stirring and left overnight at room temperature. Nanoparticles formation turns the clear solution into a white and opaque dispersion. Nanoparticles are then collected centrifuging the solution at 12500 g for 20 minutes and washed three times with EtOH. The resulting pellet was dried overnight. The dry powder was weighed and put in a Teflon bomb with 12,5 ml of EtOH and 6,25 ml of MilliQ water per gram of sample. The dispersion was left under stirring for an hour, and then put in an oven at 170°C for 16 hours for the hydrothermal treatment. After this, the powder was filtered and washed with ethanol and water and left to dry. In order to extract the surfactant, the powder was put in a flask under vacuum (0,05 mbar), in an oil bath on an hotplate at 120°C. Extraction was allowed to proceed overnight and in the end the powder was filtered and washed with EtOH and water[10].

	Molecular Weight(g/mol)	Density (g/ml)	Purity (%)	Molar Ratio
Starting solution				
EtOH	46.1	0.79	100	760.70
H_2O	18.0	1.00	100	17.04
NaF (0.1 M)	42.0	-	99	0.02
Exadecylamine	241.5	1.00	90	1.70
Precursor solution				
$Zr(OPr)_4$	327.6	1.04	70	1.00
EtOH	46.1	0.79	100	9.60

Table4.1 molar ratios of MZN synthesis

The samples were analysed by FESEM, XRD, DLS/ZP and nitrogen physisorption (BET, BJH).

4.3.2 Functionalization of MSNs with APTES

0.3 g of MSNs, gently provided by PhD Emmanuele Ambrosi and PhD Gabriele Sponchia, were dissolved in 0.25 ml of MilliQ water and 4.75 ml of EtOH under stirring. In another vial, under stirring, a solution of 0.25 ml of MilliQ water and 4.75 ml of EtOH was prepared. Glacial acetic acid was added to adjust pH to a value of 5.0. 0.3 ml of APTES (3% of the volume at the end of reaction) were added. This solution was then added dropwise to the first one, having a final volume of 10ml. Reaction was left under stirring for three hours. The resulting NPs were collected by centrifuging at 16000 g for 30 minutes and washed in MilliQ water and ethanol. The obtained pellet was dried overnight[45, 68].

These NPs were analysed by physisorption of nitrogen, DRIFT-IR, and SEM.

4.3.3 Vancomycin loading of MZNs

The protocol of drug loading is a simple impregnation process, which consists of the dispersion of a specific amount of MZNs in MilliQ water or in a buffer solution (acidic, basic or neutral), containing VCN. Particularly, used NP concentration was 20 mg/ml, antibiotic was 15 mg/ml and final volume was 0,5 ml. The solution was stirred overnight at room temperature. After the loading, NPs were separated from the solution by centrifugation (10 minutes at 12500 g). The supernatant was used to evaluate the concentration of the adsorbed antibiotic by UV-visible absorption at a wavelength of 280 nm. The drug loading amount was calculated using this equation:

Loading content (%) = (Initial amount of VCN - Residual VCN content) x 100 / amount of MZNs*

*amount and content expressed in mg

Before all tests, nanoparticles were washed once with MilliQ water in order to remove loosely bound molecules.

4.3.5 Vancomycin loading of MSNs and APS-MSNs

Based on Li et al, 2005, these experiments were conducted as paragraphs **4.3.3**.

4.3.6 Vancomycin release from MZNs

Two different types of release experiments have been executed.

The first one (Sponchia et al, 2015) consisted in the resuspension of MZNs loaded with VCN at a concentration of 0.16 mg/ml in different buffers (pH 4.6, 7.2 and 9.8) in a final volume of 18 ml. Solution was left under agitation for 24 hours. At predetermined time intervals 1 ml samples were taken, centrifuged and released vancomycin concentration was determined in the supernatant by UV-visible absorption at 280 nm.

The second method to test the release rate was based on a classical protocol (Li et al, 2005). The MZNs loaded with Vancomycin were resuspended in 2 ml of MilliQ water. This solution was transferred into a dialysis bag (MWCO = 14000 Da), and then immersed into 30 ml of PBS

solution (pH = 7.2), under gentle stirring. At predetermined time intervals, 1 ml of the exchanging buffer was collected. VCN concentration was determined by UV-visible absorption at a wavelength of 280 nm basing on the starting concentration of loaded VCN in the total volume.

Release percentage in both cases was calculated based on the starting antibiotic content, using the following formula:

Release (%) = (amount of VCN in the supernatant / starting VCN content in MZNs) x 100*

*amount and content expressed in mg

4.3.7 Bacterial strain and growth condition

The strain used for antibacterial activity tests of VCN-loaded MZNs was methicillin-susceptible *Staphylococcus aureus* ATCC 6538, gently given by ARIES s.r.l..

This strain was stored in freezer at -20°C. Starting plate was made streaking an aliquot on selective MSA medium for Gram+ bacteria and incubating it at 37°C overnight. Resulting colonies were used to inoculate both liquid cultures (growing conditions: TSB, 37°C, 200 rpm) and plate cultures (TSA, 37°C).

All this experiments were conducted under sterile conditions, in duplicate, and adding a negative control as reference.

4.3.8 Inhibition test in TSB

Firstly, test tubes were prepared adding to TSB medium increasing VCN and VCN-loaded MZN amounts (final volume = 9 ml). Overnight culture OD_{600} was determined and then test tubes were inoculated to a final OD_{600} of 0.05, corresponding to about 1.4 x 10^7 CFU/ml.

Every hour, the absorption at 600 nm was measured at UV-visible spectrophotometer in order to evaluate bacterial viability.

4.3.9 Inhibition test on TSA

OD_{600} of overnight *S. aureus* inoculum in TSB was measured and serial dilutions were made into 5 ml of TSB, in order to plate 100 – 400 CFUs. The experiments were conducted preparing TSA with different concentrations of free VCN and different concentrations of MZNs loaded with VCN. Pictures of plates were acquired with Geliance 600 Images System and then analysed with ImageJ. MIC and IC_{50} were calculated taking as a reference the negative control.

Stability of VCN-loaded MZNs over the time was also tested. Experiments were repeated after 15 and 45 days.

4.3.10 Antibiofouling activity tests

The Calgary device, a 96-well microtiter plate with PEG lids, with the kind help of PhD Emanuele Zonaro and prof. Silvia Lampis of University of Verona, was used to test antibiofouling activity of mesoporous zirconia nanoparticles loaded with VCN. Based on Harrison et al.(2006) protocol, wells containing 100 µl of nutrient broth were inoculated with the desired bacterial strains, starting from a 5 ml culture. In the case of inhibition test, *S. aureus* was directly inoculated with increasing concentrations of MZNs, VCN and VCN-loaded MZNs. Cultures were then grown for 24 hours before biofilm analysis. In the case of the eradication test, the bacteria were inoculated without any antimicrobial agents and let grow for 24 hours. Medium was then changed using increasing concentrations of the samples. The microtiter plates were put on a gyrorotary shaker at 150 rpm at 37°C for another 24 hours before biofilm viability evaluation. The growth was evaluated by plate counts[60].

The NPs were tested in a concentration range between 0 and 26 µg/ml.

To calculate the MBC from the inhibition test and the MBEC from the eradication test, PEG lids were removed and the biofilm viability was evaluated by plate counts.

4.3.11 *In vitro* biofilm formation on glass coverslips

First of all, a colony of *S. aureus* was inoculated overnight at 37°C under stirring. Six glass coverslips for each test were vertically immersed in 12 ml TBS + 1% of glucose in a beaker

with the help of a sample holder. Inoculum was made at a final OD_{600} of about 0.02. All the beakers were left overnight under stirring at 120 rpm. The tests were conducted on a mature biofilm grown for 72 h, to test the eradication activity by NPs and a 24 h biofilm, to assess the inhibition activity of biofilm by NPs. Every day the medium was changed, until the last day when the NPs were added to the medium. For each test a negative control was considered as reference. Tests were conducted inoculating VCN-loaded MZNs at a final concentration of 30 µg/ml (6 µg/ml of actual VCN).

Biofilms were briefly washed in PBS and then fixed dipping the glass coverslips for 30' at 4°C in a PBS solution containing paraformaldehyde 4%, followed by three washing steps in PBS.
Some of these coverslips were used for the analysis with CLSM and others were prepared for FE-SEM analysis.
To have an early indication of the presence of biofilm, some cover slips were stained using a blue toluidine solution.

4.3.12 Preparation of biofilm samples for FE-SEM analysis

Adapted from Vuotto and Donelli (2014) protocol, after fixation (see 4.3.11) biofilm coated coverslips for FE-SEM were prepared after dehydration with EtOH gradients and HDMS solution. Briefly, samples were washed in PBS and then immersed for 20" in solutions with increasing ethanol concentrations (10%, 30%, 50%, 70%, 80%, 90%, 96, 100%). Last step was repeated twice. After this treatment, coverslips were dipped for 20' in HDMS:EtOH solutions (1:2 and 2:1). Last washing step was repeated twice in pure HDMS. Samples were then dried and mounted on the stubs. A gold layer was finally sputtered on the stub (working parameters: 0.05 mbar, 2.5 kV, 20 mA, 120")[69].

4.3.13 Preparation of biofilm samples for CLSM

Thanks to the kind help of IOR of Bologna, bacterial cells fixed on glass coverslips (see 4.3.11) were marked with DAPI.

4.3.14 HAp shell synthesis

Adapted from Wang et al. 2005 protocol, an hydrothermal synthesis of nanorods of HAp using CTAB as cationic surfactant, the synthesis of the shell was conducted replacing the CTAB with MZNs, exploiting the well known affinity[13-18] of zirconia for phosphates. A certain amount of MZNs was put in a flask in a solution with dipotassium hydrogen phosphate buffer (pH = 12.0), in different molar ratios. Reaction was allowed to proceed for 2 hours at 50°C on an heatplate, under stirring. After this step, a solution of calcium chloride was put dropwise into starting solution and all the solution was put in a Teflon bomb for the hydrothermal treatment at 120°C for 20 hours in an oven. Eventually powder was filtered and washed with ethanol and MilliQ water[28].

Starting Salts/Solvents/NPs	**Molecular weight(g/mol)**	**Purity**	**Used quantity**	**Molar Ratio**	**mol**
K_2HPO_4*3H_2O pH = 12.0	174.18	0.99	0.140 ml	1	0.0008
H_2O	18.00	1.00	3.24 ml	231.5	0.19
$CaCl_2$	110.98	0.93	0.139 g	1.67	0.0013
H_2O	18.00	1.00	2.03 ml	139	0.11
MZNs	123.18	-	0.10 g	1	0.0008

Table4.2: molar ratios for HAp-shell synthesis

All the samples of HAp-MZNs are made changing the ratio between the quantity of precursors of hydroxyapatite and the amount of MZNs. Starting with a 1:1 HAp:MZNs ratio, as reported in Table **4.2**, the system was scaled to ratios: 1:2, 1:5, 1:10, 1:11, 1:12, 1:13.

Following experiments were conducted with the quantity corresponding to the ratio 1:10.

In the first alternative protocol, the 2 h reaction at 50°C was replaced with an overnight reaction at room temperature. In the second, the hydrothermal treatment (and also the used quantities)

was divided into two steps at 120°C of four and sixteen hours respectively, to allow all the phosphates to react with surface area of NPs.

The samples were analysed by FEG-SEM, EDS, XRPD, DLS and ZP, physisorption of nitrogen (BET, BJH) and TEM**.**

4.3.15 Vancomycin loading of HAp-MZNs

The loading of HAp-MZNs with Vancomycin was conducted as described in paragraph **4.3.3**.

4.3.16 Vancomycin release from HAp-MZNs

This experiment was conducted as explained in paragraphs **4.3.6**, using only the second method.

4.3.17 Preliminary antibacterial and antibiofouling tests

The antibacterial tests were conducted as in paragraphs **4.3.8** and **4.3.9**, with a concentration of 266 µg/ml of nanoparticles loaded with the 10% of their weight of VCN.

Also the antibiofouling activity tests were repeated with increasing concentrations of HAp-MZNs by Calgary Device, in the same conditions of paragraph **4.3.10**, both for the inhibition and eradication of biofilm formed by *S. aureus*[60].

4.3.18 Further functionalization with bis-phosphonate

Looking for possible applications of MZNs as biomaterials in orthopaedics, both MZNs and HAp-MZNs were functionalized with bis-phosphonate. Functionalization protocol requires the preparation of a solution of NPs at 10 mg/ml in MilliQ water, and the subsequent addition of the compound at a concentration of 8 mM. Reaction is allowed to proceed under stirring at room temperature for 12 hours. These nanoparticles were analysed with DLS/ZP and XPS.

4.3.19 Biocompatibility and osteogenic test

MZNs, HAp-MZNs and Hap-MZNs further functionalized with bis-phosphonate, were marked with the dye R6G in a simple impregnation process. Presence of the dye after three washes with MilliQ water was assessed by spectrofluorometric analysis.

Thanks to kind help of PhD, BSc Maria Teresa Valenti of University of Verona, all the samples were tested with the medium for MSCs cultures in a range of concentrations spanning from 5 to 100 µg/ml, using a negative control as reference[58].

5 Results and discussion

5.1 MZN characterization

MZN synthesis consisted of a neutral surfactant assisted sol-gel method[70] with the use of an inorganic salt. This is an effective process to prepare an useful system for drug delivery of MZNs and consists of using a neutral surfactant to define the pores, in combination with a salt to avoid aggregation, an hydrothermal treatment to define the shape and the extraction of the surfactant under vacuum, to avoid the pore collapse[10]. As a consequence of the many factors involved into the definition of synthesis parameters, reproducibility is a critical element.

FE-SEM analysis shows well-defined spherical nanoparticles. Different synthesis batches gave an overall mean diameter of 400 ± 100 nm. DLS measures confirmed these dimensions. Figure **5.1** shows representative images of synthesized batches.

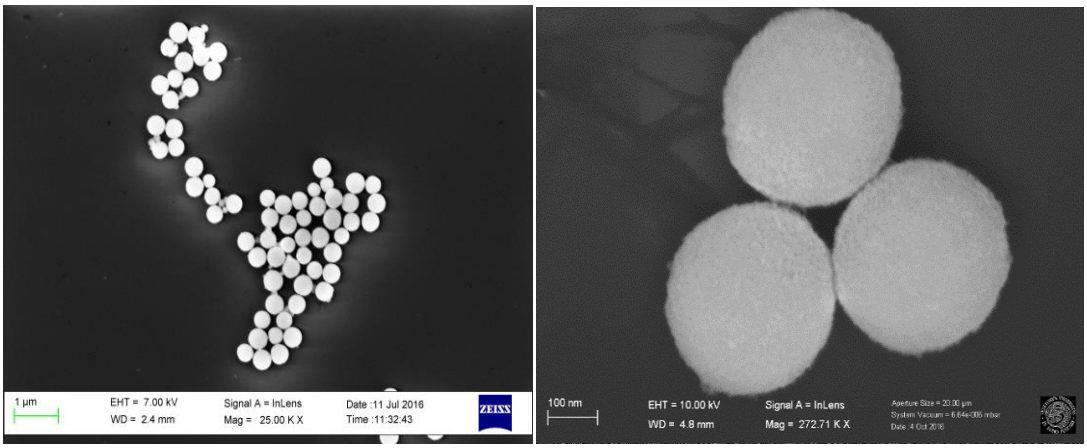

Figure 5.1 FE-SEM images of MZNs. On the left, the image shows the uniformity in shape and dimension of the sample. On the right, the image shows the slight surface roughness of NPs, probably due to the porosity of MZNs or to the presence of crystallites that form the NPs (see XRD analyses).

Figure **5.2** shows a representative N_2 adsorption–desorption isotherm of the type IV, based on the "Brunauer (or BDDT) classification" with a H1 hysteresis loop, according to the IUPAC classification, typical for mesoporous systems. The samples have a specific surface area of 210.6 ± 20 m^2/g, and a pore diameter of 4.92 ± 0.20 nm, according to the BJH model applied on the adsorption branch. The pore volume is about 0.31 ± 0.02 cm^3/g. Figure s **5.2** and **5.3** show an example of physisorption analysis of a batch of MZNs.

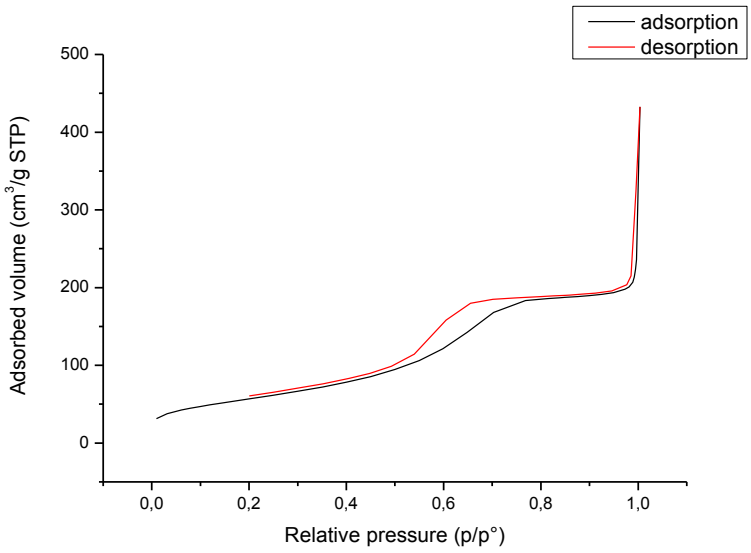

Figure 5.2 N_2 physisorption curve of MZNs that shows an isotherm of type IV, typical of mesoporous systems

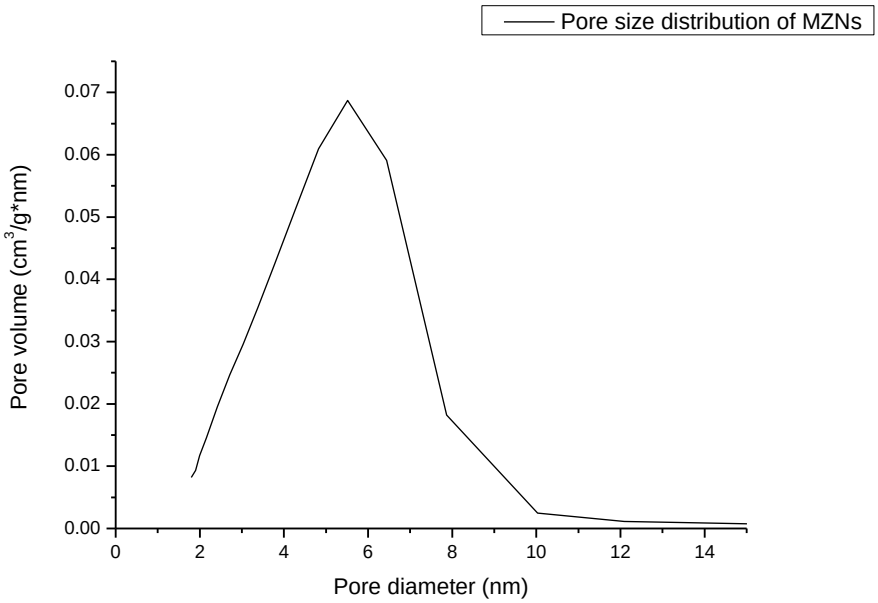

Figure 5.3 Pore size distribution of MZNs, adsorption BJH.

Zeta potential of NPs influences their stability and depends on the pH of the solution. ZP measurements in figure **5.4** show the surface charge depending on pH. At low pH values, the ZP of MZNs is positive (25 – 30 mV). Isoelectric point falls in the range between 6.0 and 7.0. At higher pH values ZP becomes negative, reaching a plateau of about -30 mV at pH = 10.0.

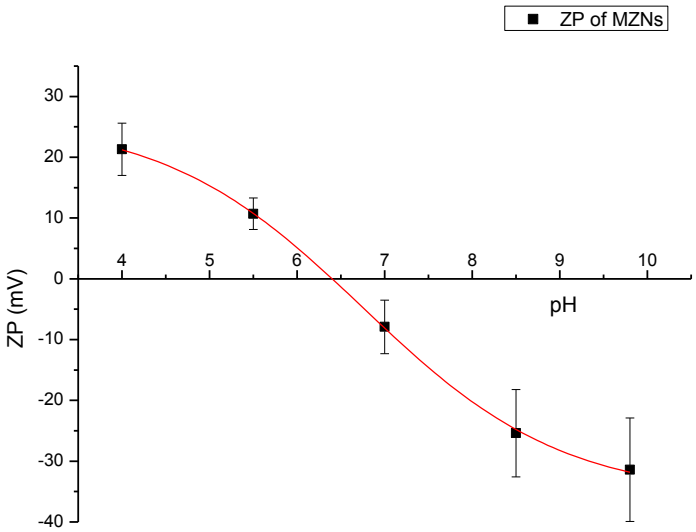

Figure 5.4 Zeta Potential of MZNs as function of pH. At low pH values MZN surface charge is positive and become negative at high pH values. The isoelectric point falls between 6.0 and 7.0.

5.2 APS-MSN characterization

MSN were gently provided by PhD Ambrosi and PhD Sponchia. Nanoparticles were opportunely functionalized with APTES, to compare MZN loading with a well-know DDS loading, basing on Li et al. 2015.

These nanoparticles are spherical and with a mean diameter of 157 ± 40 nm (see fig. **5.5**).

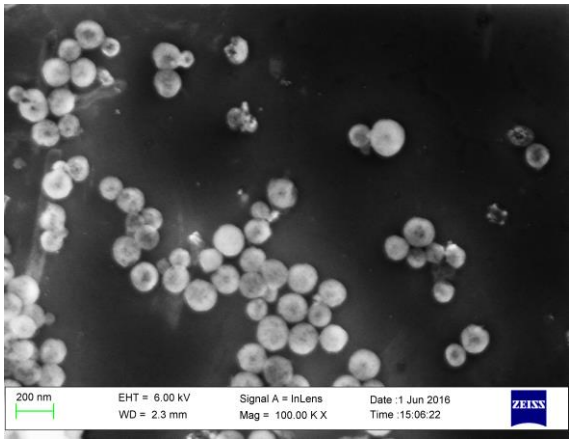

Figure 5.5 FEG-SEM image of MSNs that shows a inhomogeneous batch of spherical NPs.

The N_2 adsorption–desorption isotherm of type IV in fig. **5.6** confirms the mesoporosity of the MSNs. These nanoparticles have an high surface area of 950 m^2/g and average pore diameter of 5 ± 0.6 nm.

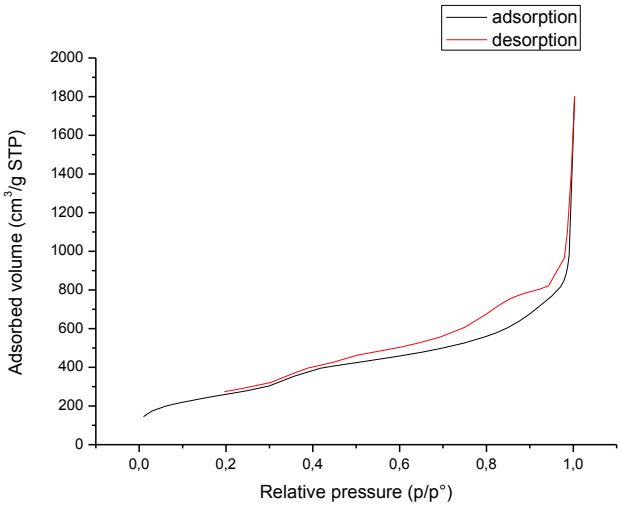

Figure 5.6 N_2 physisorption of MSNs, that shows an isotherm of type IV, typical of mesoporous systems

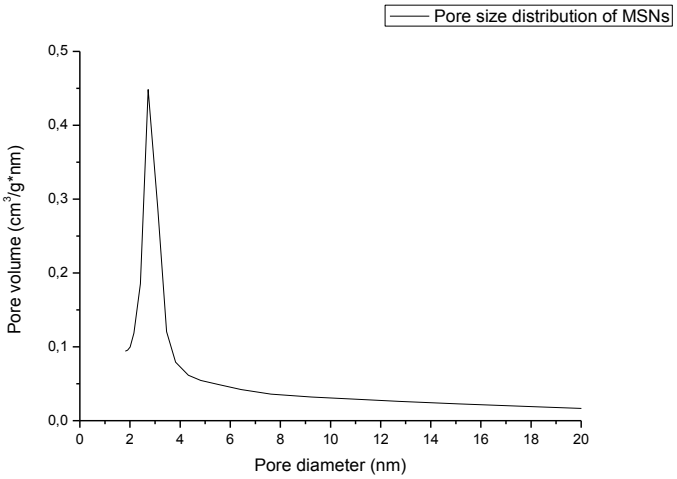

Figure 5.7 Pore size distribution of MSNs, BJH adsorption. Even if the most of NPs have a diameter around 3 nm, the average is influenced by high values and is about 5 nm.

DRIFT-IR analysis in Fig. **5.8** shows the occurred post grafting functionalization obtained by Hermanson protocol[68]. The range between 1200 and 400 cm^{-1} are typical of the silanes and it is present in both the spectra. The peak at about 3700 cm^{-1} refers to the stretching of OH bonds, that are on the surface of NPs before the functionalization and that disappear when the APTES moiety is grafted onto the surface. The peak at about 3000 cm^{-1} of APS-MSNs corresponds to the stretching of saturated CH bond. The peaks from 1600-1700 to 1200 cm^{-1} are related to the amino-groups of the APTES molecules.

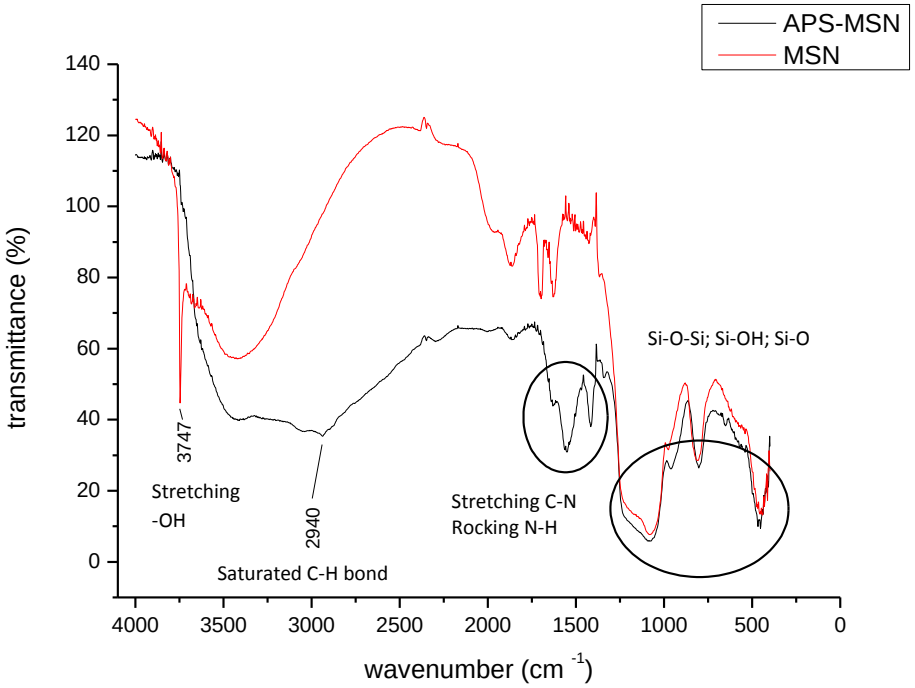

Figure 5.8 DRIFT-IR spectra of MSNs and APS-MSNs, that show the main groups proving the functionalization with APTES.

5.3 HAp-MZN characterization

HAp-MZN synthesis consisted of an hydrothermal treatment, adapted from Wang et al. (2005)[28], replacing the surfactant with MZNs. This reaction aims to coat nanoparticles with an HAp shell, for possible application in orthopaedics. Starting with an initial molar ratio of 1:1 between HAp precursors and MZNs, serial experiments were conducted to synthesize a well-defined shell, reducing as much as possible the formation of unbound HAp crystals. To do so, experiments with different HAp : MZNs molar ratios (1:2, 1:5, 1:10, 1:11, 1:12 and 1:13) and under different conditions of temperature were conducted and compared.

FE-SEM images show well-defined spherical nanoparticles of ZrO_2 surrounded by crystals of hydroxyapatite. Because of P and Ca are much less heavy elements than Zr, SEM images were collected using different accelerating voltages: 2.5 kV and 12.5 kV or 20 kV, to observe the presence of the crystals.

Figures below show the most significant samples. Experiments with molar ratio lower than 1:10 don't show relevant differences.

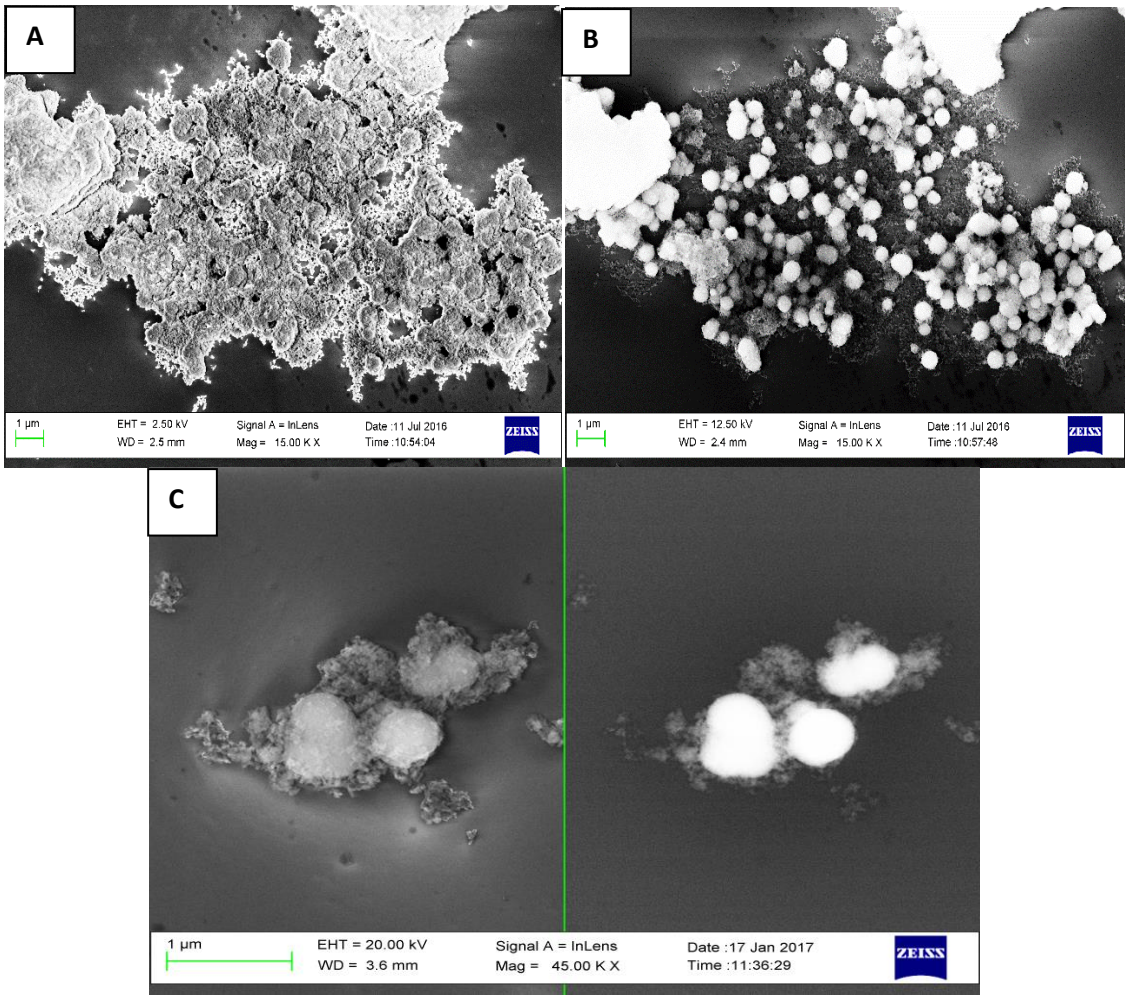

Figure 5.9 HAp-MZNs, ratio 1:1. **A**: 2.5 kV. **B**: 12.5 kV. The lower applied voltage allow to have information about the surface details. On the contrary, higher voltages highlight inner structure features: in this case it is possible to see MZN cores. **C:** 20 kV images of HAp-MZNs with acquisition signals, on the left secondary electrons, on the right backscattered electrons. It is possible to notice the different sample density.

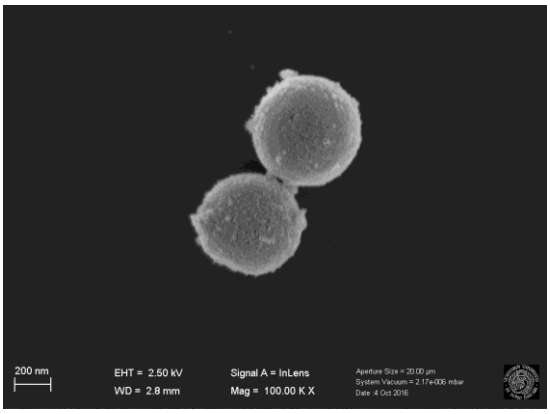

Figure 5.10 HAp-MZNs, ratio 1:2

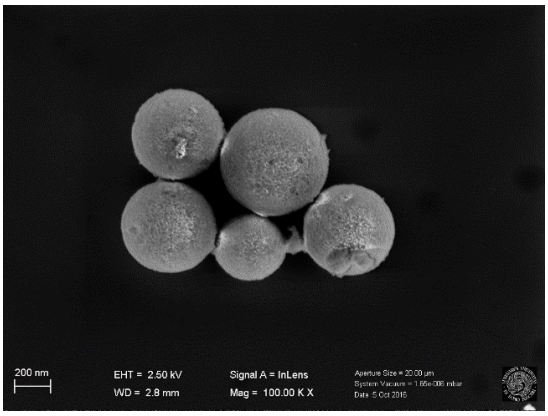

Figure 5.11 HAp-MZNs, ratio 1:5

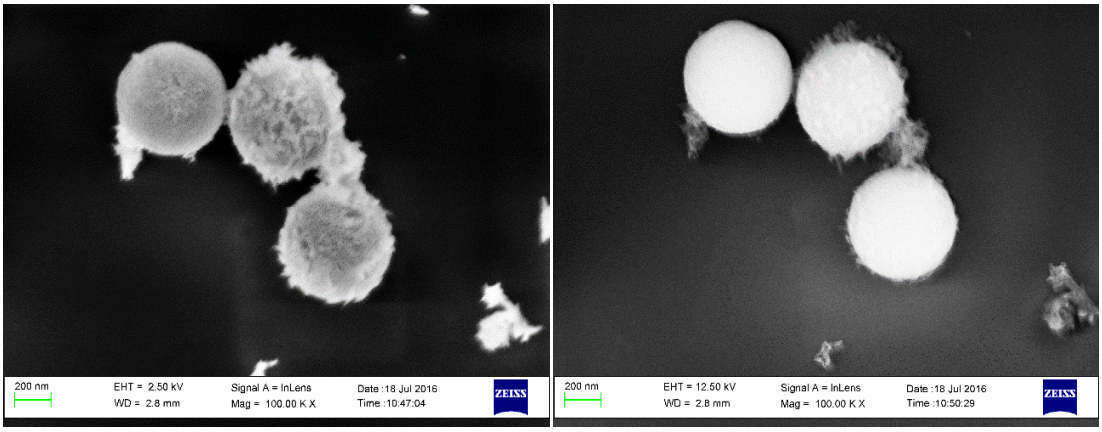

Figure 5.12 HAp-MZNs, ratio 1:10. **On the left**: 2.5 kV. **On the right**: 12.5 kV. The increment of the diameter due to the presence of the Hap shell is about 50 nm.

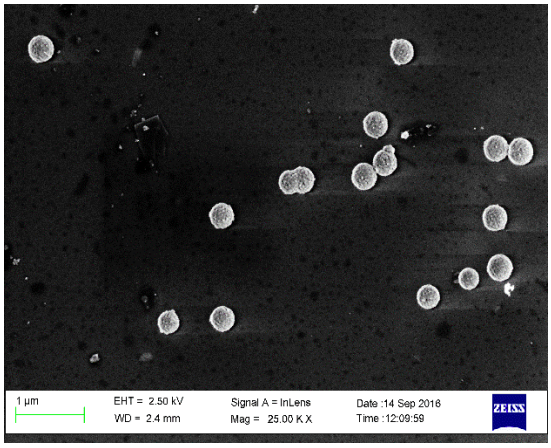

Figure 5.13 HAp- MZNs, ratio 1:13

As described in paragraph **4.3.14**, some variations of the starting protocol have been made in order to understand how synthesis parameters can improve resulting HAp shells. In the first case, the synthesis was conducted at room temperature to exploit the affinity of phosphates and zirconia. On the other hand, to allow to all HAp precursors to react with NPs without using any surfactants or salts to control the reaction outcome, different steps of hydrothermal treatment were performed. Figure **5.14** on the left shows HAp-MZNs synthesized at room temperature, without the initial reaction at 50°C. The resulting NPs probably have crystals on the surface, but the batch is not so homogeneous as previous experiments. Probably the starting reaction is necessary to ensure a cooperative interaction and a direct binding between the phosphate precursor and NPs, thus allowing the growth of a well-defined shell of HAp. On the right of figure **5.14**, it is represented the batch of HAp-MZNs synthesized with several. This batch shows less uncoupled HAp crystals than the batch synthesized without the initial reaction at 50°C. In fact, it is more uniform and some crystals are also visible on the NP surface. Despite this, nanoparticles result more aggregated than batches shown in figures **5.10**-**5.13**. This behaviour probably depends on different synthesis parameters, such as low precursor concentrations and high temperature, which seem to promote NP aggregation. Since the high temperature is needed, in order to avoid this problem, an higher precursor concentration could be useful in the first reaction step.

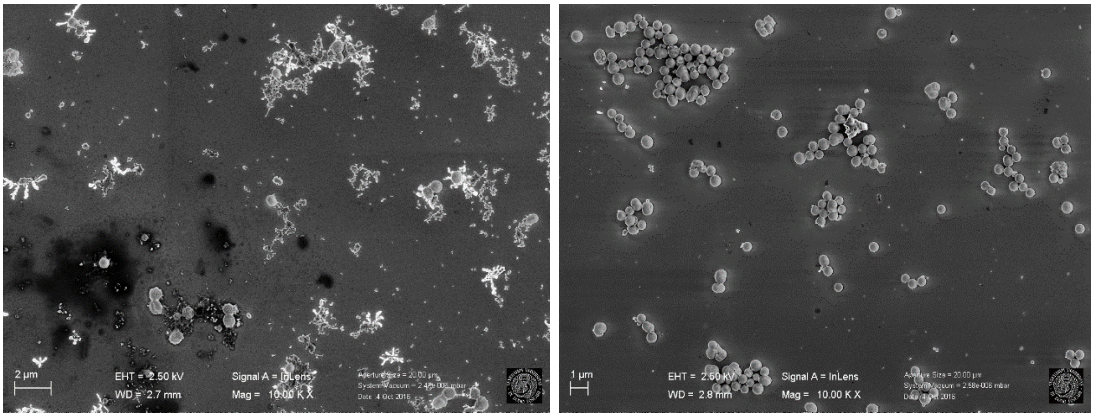

Figure 5.14 HAp-MZNs, ratio 1:10. **On the left**: synthesized at room temperature. The picture shows an inhomogeneous sample. **On the right**: synthesized by different steps of hydrothermal treatment. The figure shows more aggregation between NPs.

The SEM-microanalysis shows the presence of calcium, but the zirconium peak covers the phosphorus signal, so it is impossible to assess its presence.

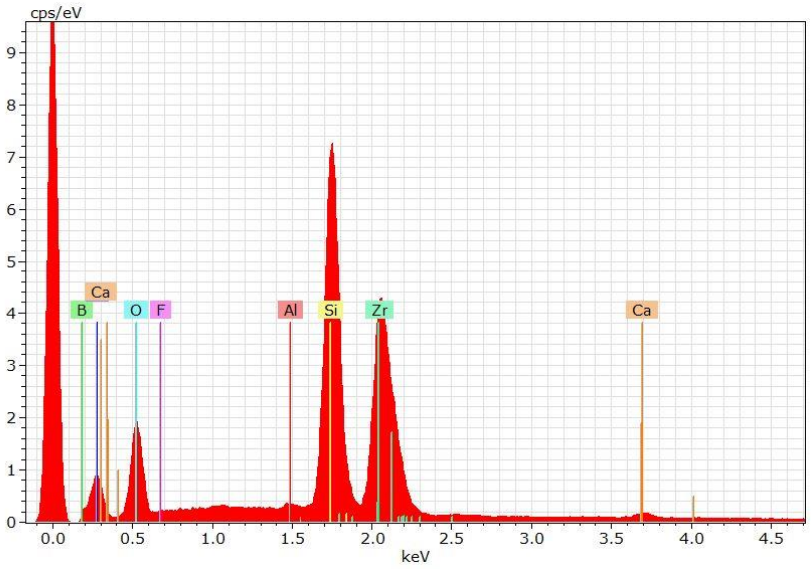

Figure 5.15 EDX analysis of HAp-MZNs, that shows the presence of Ca in the sample. The Zr peak covers the P signal.

XRPD measurements confirm the presence of orientated crystals of HAp on the direction 001, as shown from Rietveld analysis. However, the presence of crystals is evident in the XRD analysis just for the batch with higher HAp concentration. Simulations of diffractograms in figure **5.16** confirm that only the XRD pattern of HAp-MZNs where the quantities of HAp precursors and MZNs are the same should show the presence of hexagonal phase of hydroxyapatite. The batches with ratio of 1:5 or 1:10 between HAp precursors and MZNs don't show the hexagonal phase of HAp, both in simulation and in experimental data.

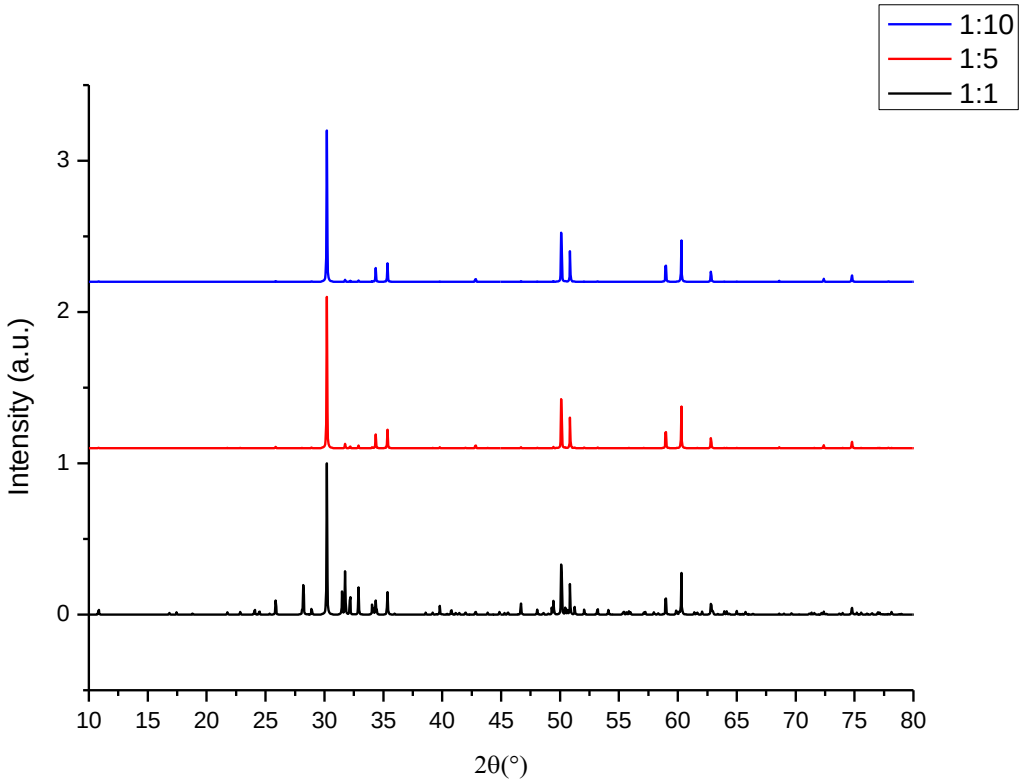

Figure 5.16 XRPD simulation data of HAp-MZNs, ratio 1:10, 1:5, 1:1. Only the results corresponding to HAp-MZNs with higher concentration of HAp (black curve) show the presence of its hexagonal phase.

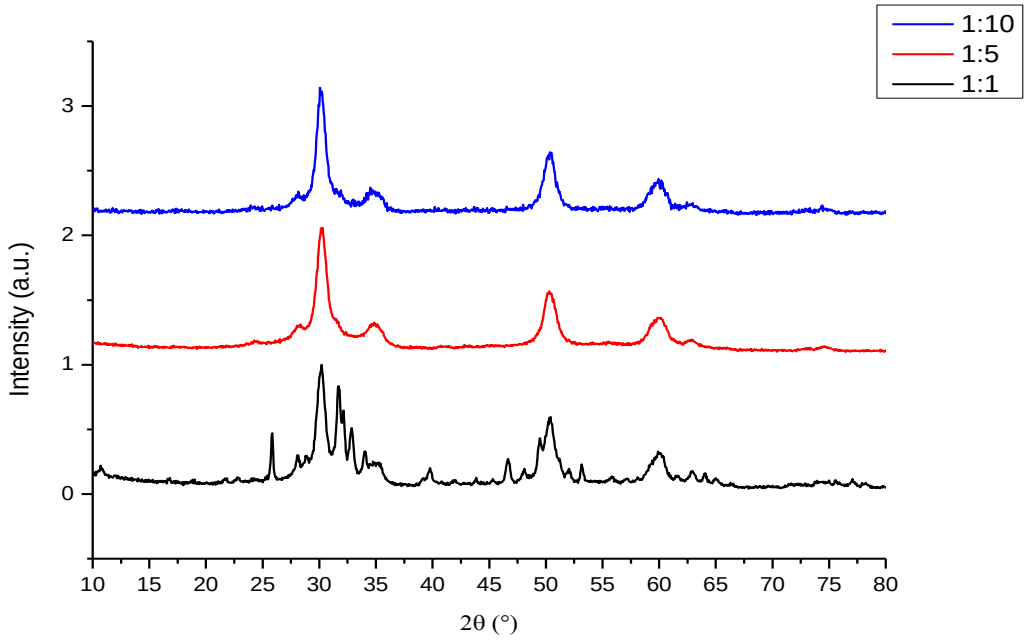

Figure 5.17 XRPD experimental data of HAp-MZNs, ratio 1:10, 1:5 and 1:1. As expected from simulations, the only HAp-MZN pattern showing hexagonal phase of HAp is the last one (black curve), corresponding to the higher HAp:MZNs ratio.

As expected, Rietveld fits of samples, as in figures **5.19** and **5.20** don't show the hexagonal phase of HAp (ICSD 56307), differently from figure **5.18**. Probably, this depends on the weight of zirconium, heavier than other elements and its quantity compared to HAp amount. In these following three figures, the fit of every sample is reported, with the difference between the experimental and calculated data. The quantitative analyses of the phases, calculated from lattice parameters, are reported in Table .. . About the MZNs, a percentage of amorphous phase is present, as expected from Sponchia et al. (2015), but there are also the tetragonal (ICSD 164862) and monoclinic (ICSD 417639) polymorphs. This, probably, depends on what is described in Dapiaggi et al. (2010)[71], about zirconium oxide NPs that are crystalline under a certain dimensions. MZNs shouldn't be crystalline under 1170°C. From the analysis of dimensions, executed using Warren-Averbach equation, in Table **5.1**, the crystallites that represent all different phases have dimension under 10 nm of diameter. The MZNs could thus be polycrystalline spheres with porous channels inside.

Quantitative analysis				
	Tetragonal ZrO_2	**Monoclinic ZrO_2**	**Amorphous ZrO_2**	**$Ca_5(PO_4)_3OH$**
HAp : MZNs	**%**			
1:1	28	14	0	58
1:5	17	56	27	0
1:10	9	25	66	0
Size				
HAp : MZNs	**nm**			
1:1	8.0	3.2		23
1:5	8.1	6.1		0
1:10	8.4	5.1		0

Table5.1 Quantitative analysis and size calculation from diffractograms of HAp-MZNs

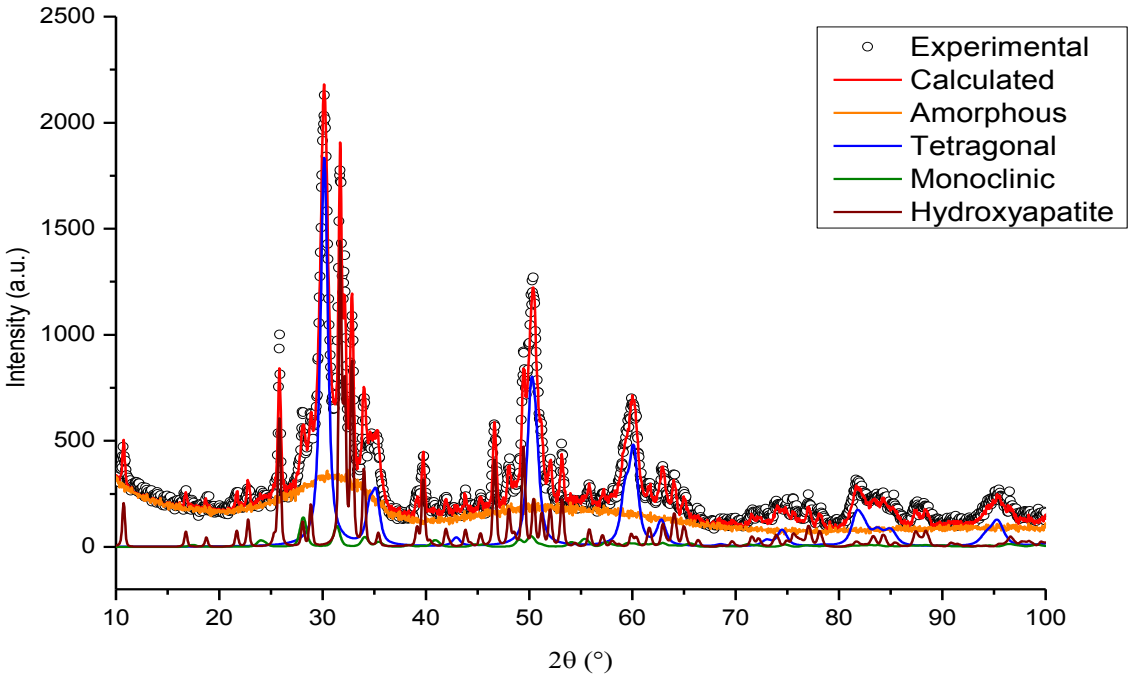

Figure 5.18 Rietveld fit of HAp-MZN XRPD analysis with all phases of the sample, ratio 1:1. This is the only batches that shows hexagonal phase into XRD analysis.

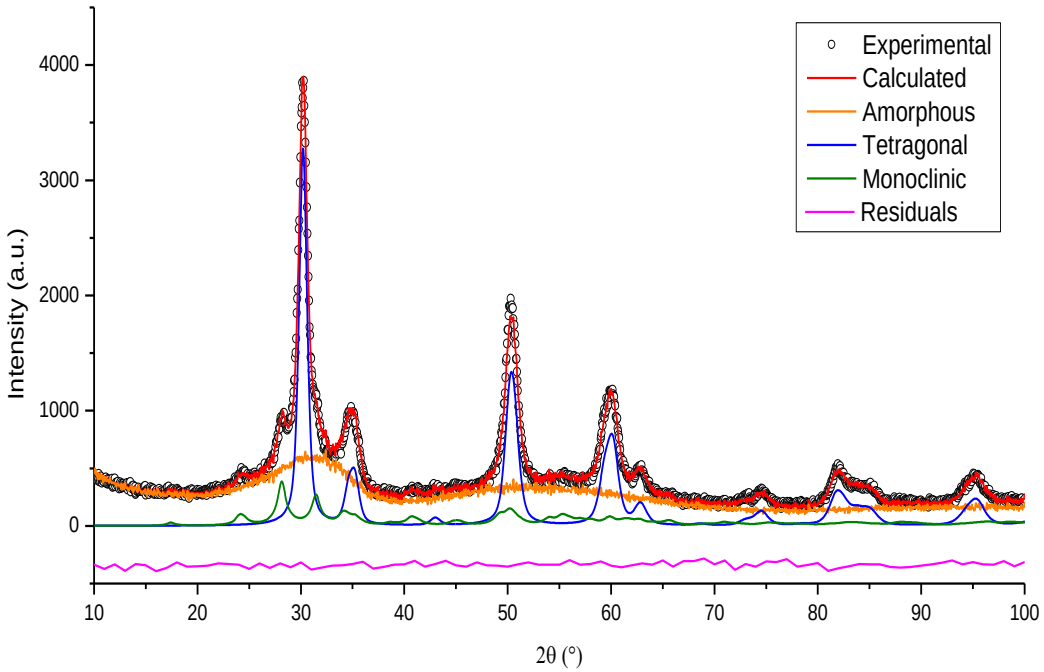

Figure 5.19 Rietveld fit of HAp-MZN XRPD analysis with all phases of the sample, ratio 1:5. The presence of HAp phase is not detected.

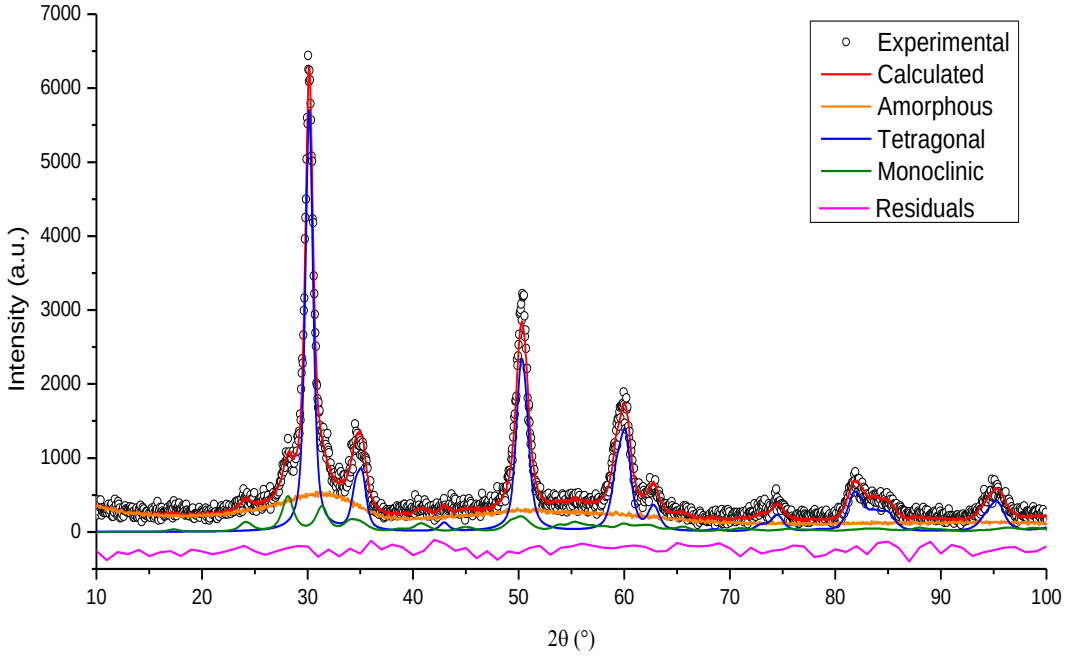

Figure 5.20 Rietveld fit of HAp-MZN XRPD analysis with all phases of the sample, ratio 1:10. The presence of HAp phase is not detected.

TEM analyses show the most representative sample, as described in paragraph **4.3.14**, with the ratio 1:10 between precursors of HAp and MZNs. These analyses were conducted to confirm the presence of HAp crystals around NPs. HRTEM images represent the region around NPs and confirm the presence of crystallites. SAED analyses show the presence of HAp on crystallites, based on ICDD 740566[72].

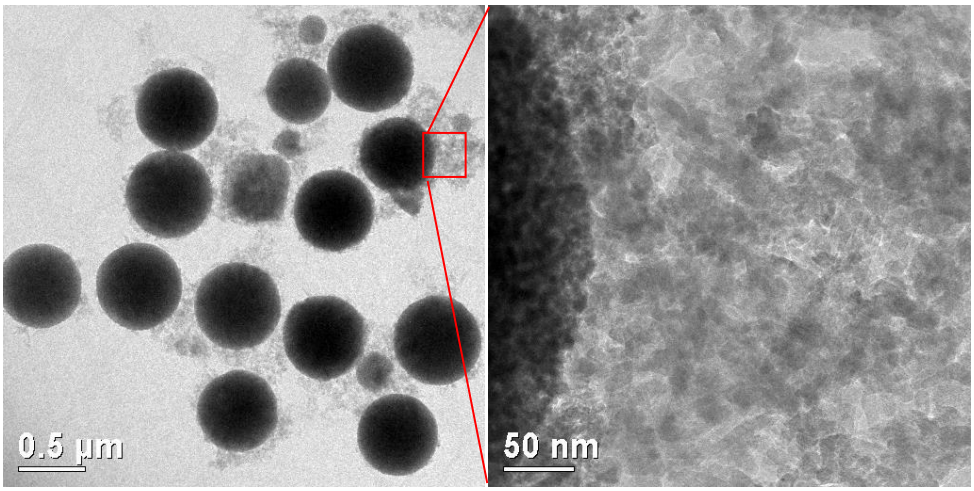

Figure 5.21 TEM images of HAp-MZNs, ratio 1:10. Picture on the right is a magnification of a region of the picture on the left. The different density between HAp and MZN is visible.

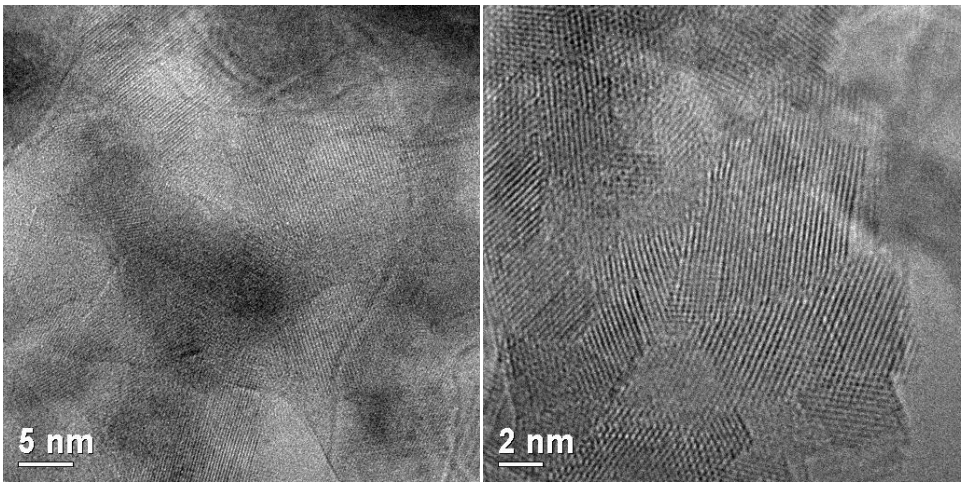

Figure 5.22 HRTEM images of HAp-MZNs, ratio 1:10. The crystallites of HAp are visible in these pictures, especially on the right.

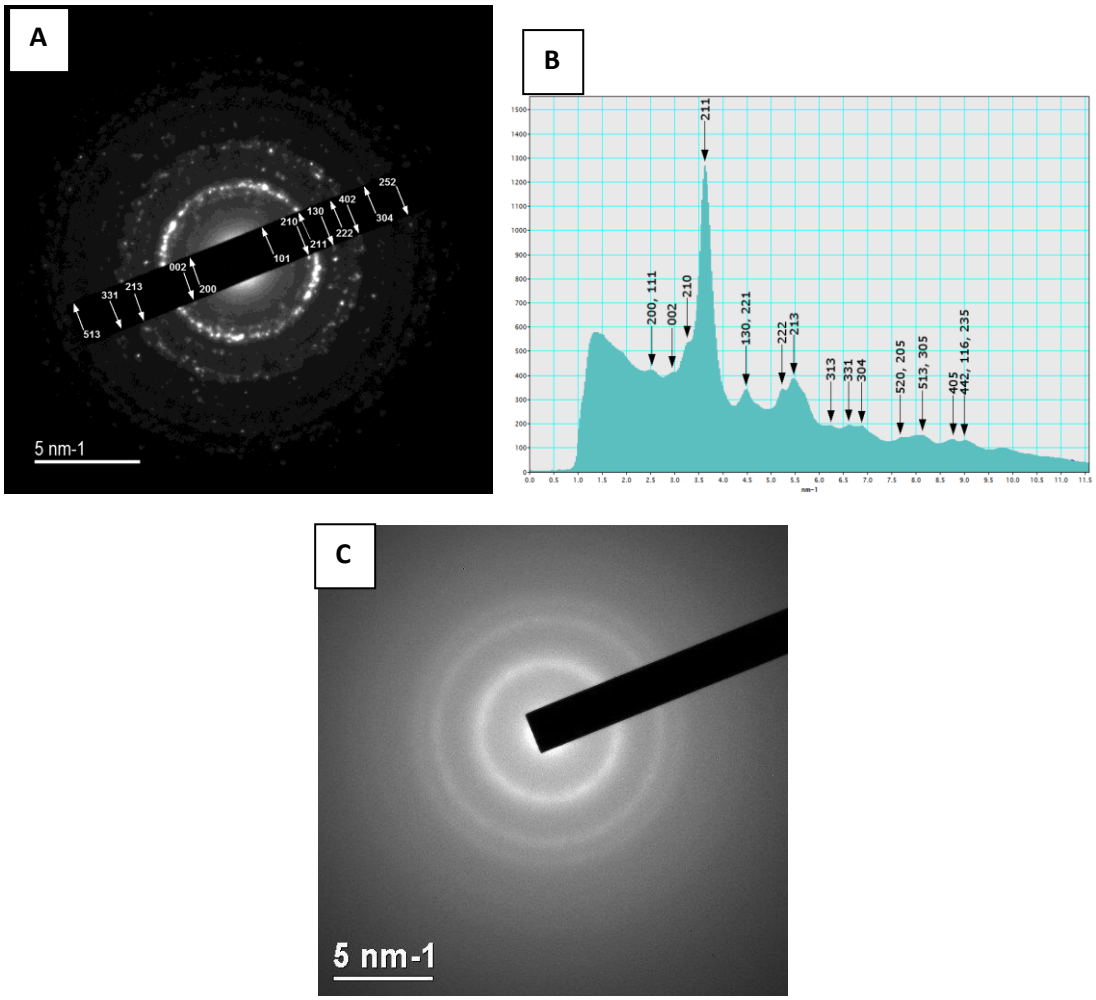

Figure 5.23 SAED analyses of HAp-MZNs, ratio 1:10. **On the top:** SAED (**A**) of region around MZNs and its corresponding intensity profile (**B**), that confirm the presence of HAp on the surface of NPs. **On the bottom: (C)** SAED of the region corresponding to MZNs, that shows different phases in addition to the hexagonal phase of Hap.

EDX-TEM analyses in Fig. **5.24** confirm the presence of P and Ca around NPs. In the region corresponding to MZNs, Zr peak overlays P signal, but the presence of Ca is validated. This difference from EDX-SEM analyses depends on both the TEM capability to select a smaller area for the microanalyses and the absence of a bulk support for TEM samples, which would contribute to the spectrum detected.

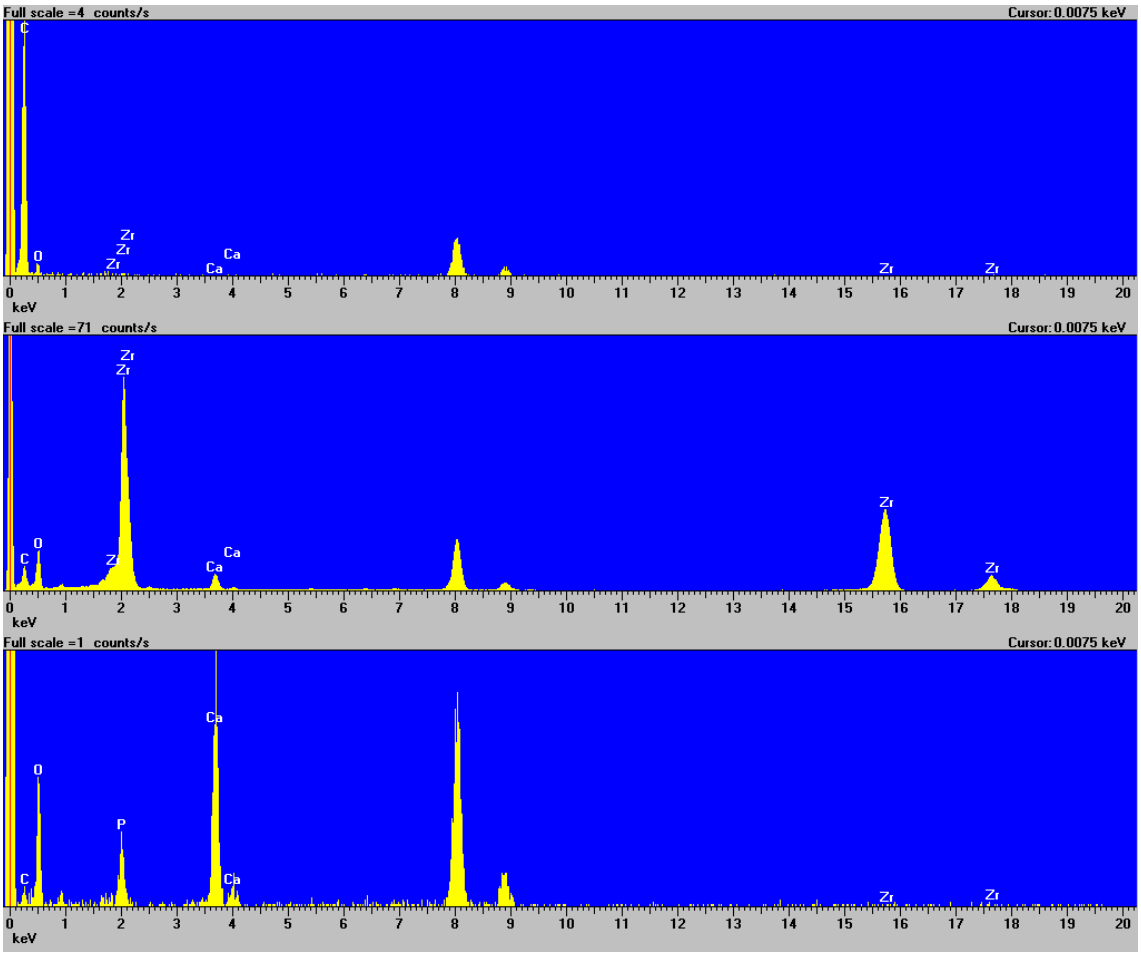

Figure 5.24 EDX-TEM analyses of HAp-MZNs. **On the top**: control, TEM sample holder. **Centre**: region of a MZNs. **On the bottom:** region around NPs. This last analysis shows both the presences of P and Ca.

ZP measurements don't show relevant differences with the uncoated MZNs.

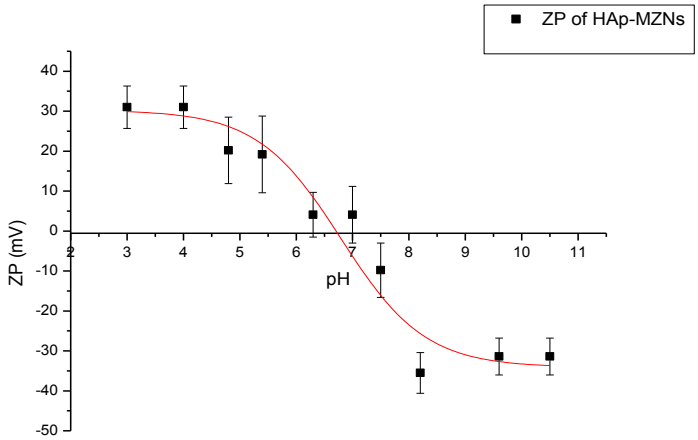

Figure 5.25 Zeta Potential of HAp-MZNs as function of pH. These measurements have not relevant differences from MZN ZP.

Figure **5.26** shows a representative N_2 adsorption–desorption isotherm of the type IV, typical of mesoporous materials. The nanoparticles with HAp have a surface area of 148.3 ± 13 m^2/g, lower than starting MZN surface area, because of the presence of HAp crystals. The distribution of pore size (Fig. ..) shows an average pore diameter of 5.31 ± 0.1 nm, higher than MZN average pore diameter. Probably HAp crystals close smaller pores. The pore volume is about 0.25 ± 0.1 cm^3/g. Figure **5.26** and **5.27** show an example of physisorption analysis of a batch of HAp-MZNs.

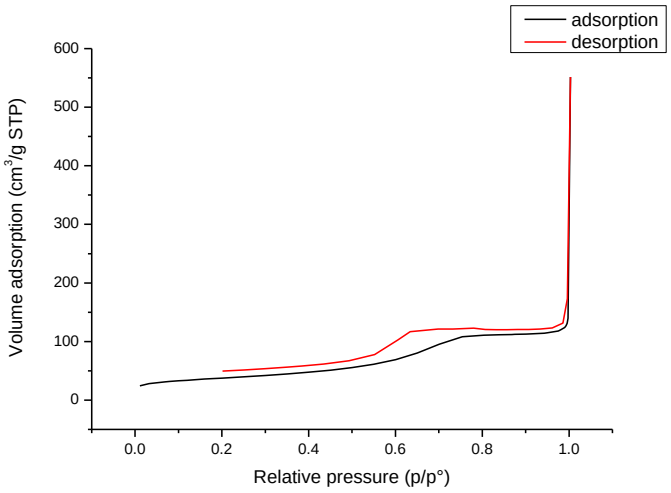

Figure 5.26 N_2 physisorption curve of HAp-MZNs that shows the typical isotherm of type IV of mesoporous systems.

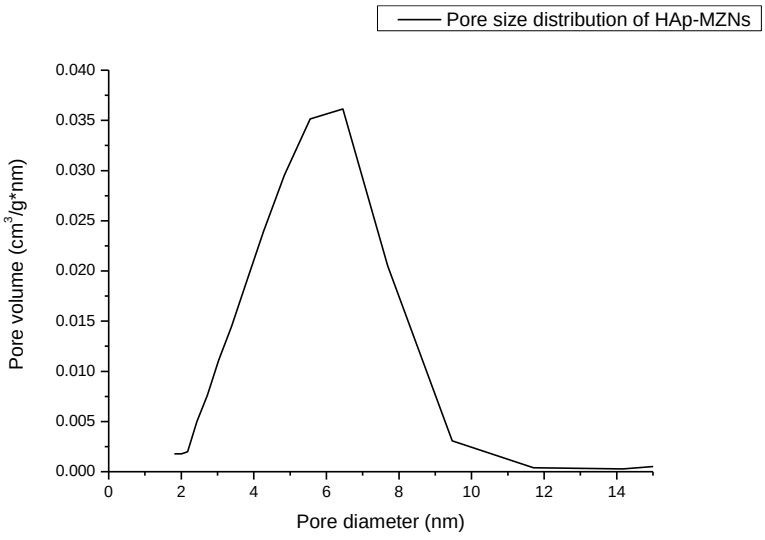

Figure5.27 Pore size distribution of HAp-MZNs. The average diameter is around 5 nm.

5.3.1 Further functionalization with bis-phosphonate

Figure **5.28** represents the ZP of MZNs functionalized with a bis-phosphonate, using the note affinity of zirconium(IV) oxide and phosphates. It's possible to note that surface charge of modified MZNs doesn't show positive values, even at low pH. The ZP measurements of HAp-MZNs don't show relevant differences from unmodified MZNs. From these changes in surface charge it's possible to deduce that the bis-phosphonate modifies NP surface. This affinity could be exploited to modify MZN surface for different kind of applications. These phosphates/phosphonates could be used as linker between MZNs and a medical device surface or as therapeutic agents or as cross linker with other molecules, too.

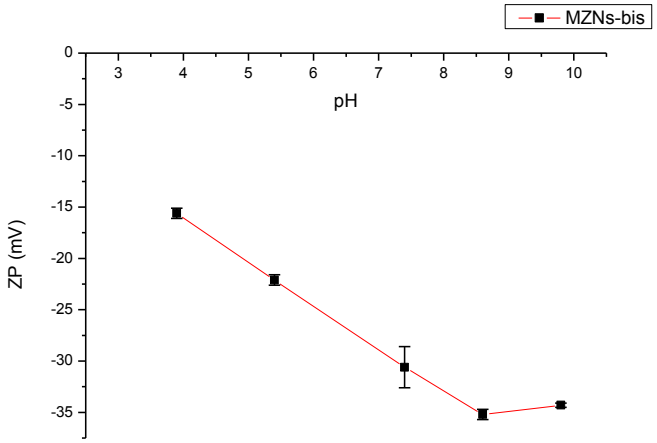

Figure 5.28 Zeta Potential of MZNs functionalized with bis-phosphonate. The presence of this molecule on the surface of NPs is confirmed by the more negative surface charge at low pH values.

5.4 VCN loading

The protocol used for the loading of VCN into the NPs was an impregnation process. Knowing the structural parameters of the system, such as the dimensions of the antibiotic and the pore volume of nanoparticles, the maximum theoretical loading efficiency was calculated*.

*VCN dimensions: 1.5 nm x 2.5 nm x 1.0 nm = 4 nm3,
VCN molecular weight: 1449.3 g/mol,
MZN pore volume: 0.31 cm3/g.
Used equations:
Max VCN molecules = NP pore volume / VCN volume
VCN mol = Max VCN molecules / Avogadro constant
Corresponding VCN mass = VCN mol * VCN molecular weight
Max theoretical efficiency = VCN mass * 100

The maximum theoretical loading efficiency in the case of MZNs is about 20% of their weight. So, all kind of used NPs (MZNs, HAp-MZNs, MSNs, APS-MSNs) had the same pore dimensions. Different conditions were used for loading, as shown in Tab **5.2**. Ideal parameters of loading have been found. NPs were at concentration of 20 mg/ml and VCN at 15 mg/ml, in a final volume of 0.5 ml, under vigorous stirring. MZNs show a great affinity with the antibiotic in MilliQ water and in neutral or acidic buffer. In a basic buffer MZNs don't load the antibiotic. This probably depends on the surface charge of nanoparticles, changing as function of external pH, as shown with ZP measurements (see figure **5.4**) . Based on Takacs-Novak et al. (1993)[73] studies on dependence of VCN acid-base properties, it is possible to follow the antibiotic net charge: as you can see in figure **5.29**, at high pH value both MZNs and VCN have high negative charge, which prevents the loading. Around neutrality, the two components have opposite charges and can thus interact. At low pH values, the presence of Cl^- probably masks some of the positive charges in the system, allowing the loading results obtained.

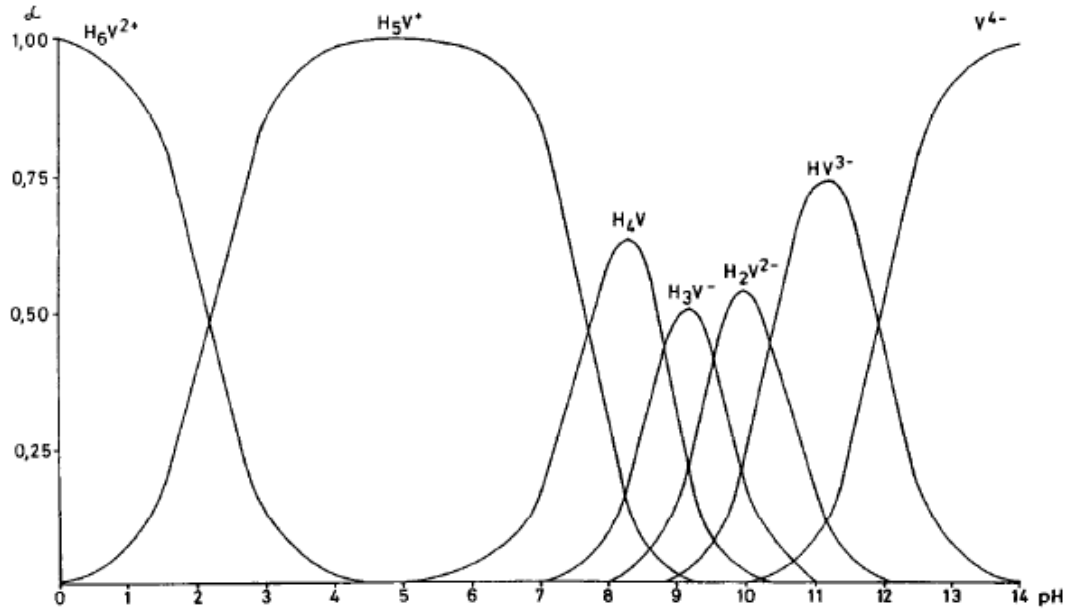

Figure 5.29: Distribution of VCN macrospecies as function of pH values (Takacs-Novak et al.,1993). Generally, the VCN is positive at acidic and neutral pH values and negative at basic values. The isoelectric point falls at about 8.0.

HAp-MZNs show a loading efficiency about the half respect to unmodified MZNs, probably because of both the presence of something on the surface which hampers the loading and a smaller pore dimension. Despite of the same pore diameter and the higher density of MZNs respect to MSNs, the last system doesn't load VCN. APS-MSNs[45] have a loading efficiency in MilliQ of about 2%, probably because APTES moieties show their terminal amino group, creating a repulsion force with amino groups of VCN. This shows different outcomes from how reported on Li et al. 2005[45]. In order to load this antibiotic, MSNs could need different

functionalizations, with other silanes that present terminal carboxyl groups which can improve their affinity with the drug.

NPs	Solvent/ Buffer	Loading Efficiency %	St. Deviation	N
MZNs	MilliQ	24.0	9.0	20
	pH 4.6	14.0	8.0	3
	pH 5.4 NaCl 80 mM	15.5	6.0	3
	pH 6.9	22.5	2.0	3
	pH 9.8	0.0	0.0	3
HAp-MZNs	MilliQ	11.7	5.5	3
MSNs	MilliQ	0.0	0.0	3
APS-MSNs	MilliQ	2.0	0.5	3

Table 5.2 VCN loading of NPs, N = number of independent loading tests

A TGA measurement was executed, to validate UV-Vis measurements. The analyzed sample UV-Vis and TGA measurements of the analyzed sample gave the same results (about 10 % of loading efficiency).

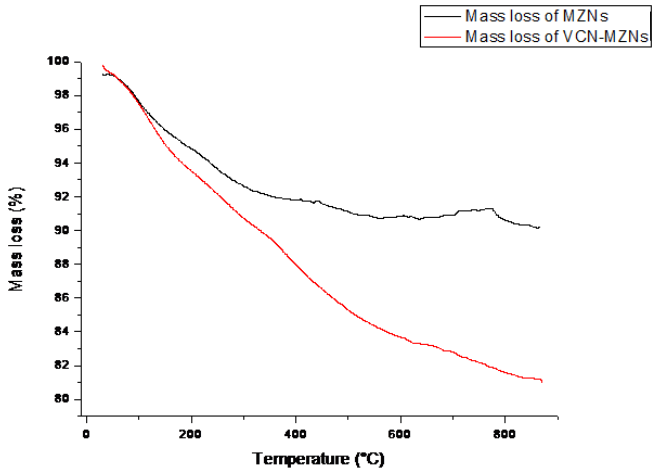

Figure 5.30 TGA of VCN-Loaded MZNs. The difference between the mass loss of loaded and unloaded NPs is about 10% of their weight.

5.5 VCN release

VCN release tests were conducted in two ways, as described in paragraph **4.3.6**.

Figure **5.31** shows released concentrations of VCN by MZNs in different time and in different buffer solutions. At pH 9.8 all drug is released in about 300 minutes, having the release of more than an half of the antibiotic in first 200 minutes. At acidic and neutral pH all VCN is released between 1200 and 1400 minutes. The dependence of drug release on pH values could be exploited for different applications of MZNs.

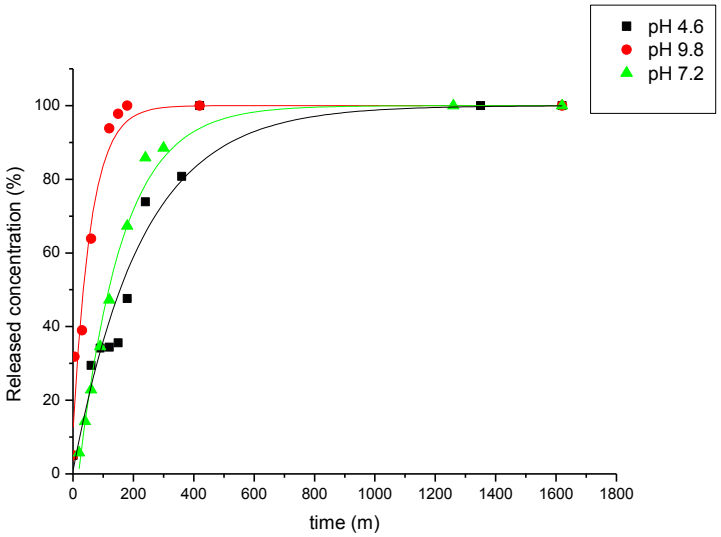

Figure 5.31 Release tests of VCN-loaded MZNs at different pH values. MZNs show different release rate of VCN. As expected from loading data, in basic buffer the release is faster than other buffers.

The second method used to test the release of NPs was described in paragraph **4.3.6** .

Results between MZNs and HAp-MZNs were collected and compared. As expected from the loading of NPs, the presence of HAp crystals on the surface of NPs slows down the release process, as shown in figure **5.32**.

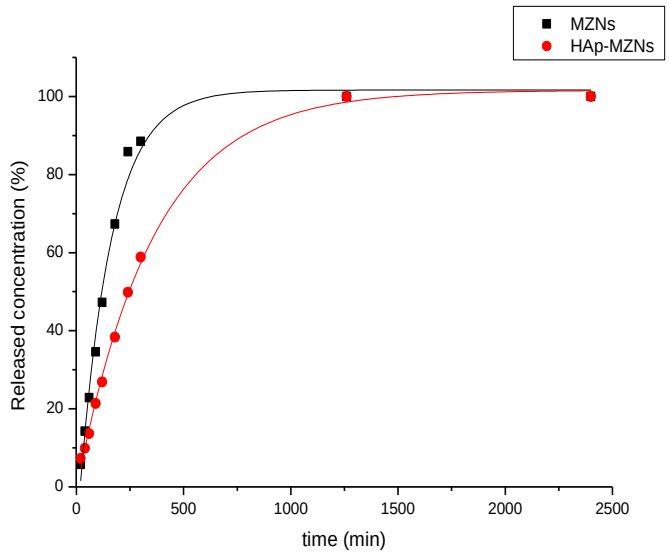

Figure 5.32 Release tests comparison between MZNs and HAp-MZNs. The presence of HAp on the surface of MZNs slows down drug release.

Figure **5.33** shows the release rate, adapted from Higuchi model, of both NPs, : it is possible to appreciateto underline the slower release rate of HAp-MZNs than MZNs (Dash et al. 2010)[74]. This can influence the pharmacokinetics, biodistribution and therapeutic activity.

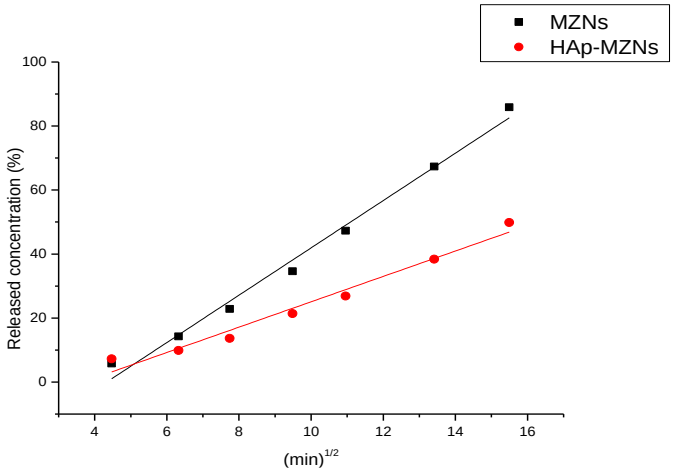

Figure 5.33 Comparison of the release rates of MZNs and HAp-MZNs, adapted from Higuchi model, as function of square root the time.

5.6 Inhibition tests in TSB

The effectiveness of VCN-loaded NPs was firstly tested in liquid medium. Both free drug and encapsulated drug were tested. About free drug, resulting data confirmed what reported in literature[35]. The MIC is around 1 µg/ml, as shown in figure **5.34**. Looking to growth curve of *S. aureus* ATCC 6538, the lowest reported concentration of 0.57 µg/ml only delays the exponential phase respect to control. Otherwise, the highest reported concentration of 1.13 µg/ml is lethal for the strain.

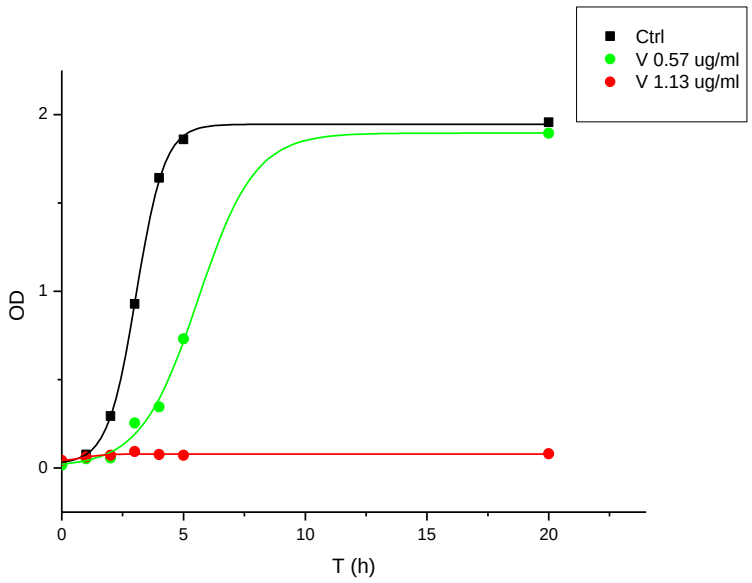

Figure 5.34 VCN inhibition test in TSB of *S. aureus* ATCC 6538. The black curve represents the negative control without VCN. The green represents the lowest concentration of VCN that only delays the bacterial growth. The red one shows the highest concentration of VCN, lethal for the strain. The MIC value is obtained from the comparison of these curves.

Different increasing concentrations of VCN-loaded MZNs were also tested. The concentrations in figure **5.35** refer to MZNs. The batches used in these experiments were loaded with 20% of their weight with the antibiotic. From these data, VCN-loaded NPs seem to work less than free drug. This probably depends on the type of the test. It was conducted in liquid medium and there are many factors to consider. Firstly, the OD measurements don't distinguish between dead or alive cells and it can be influenced by the scattering of NPs. Furthermore, this type of experiments starts with a known initial concentration of bacteria and in a liquid medium, cells have the possibility to reproduce even after the depletion of the drug.

The MIC seems to be included spanning in a range between 9 and 30 µg/ml, corresponding to a VCN concentration of 1.8 – 6 µg/ml (see fig. **5.35**).

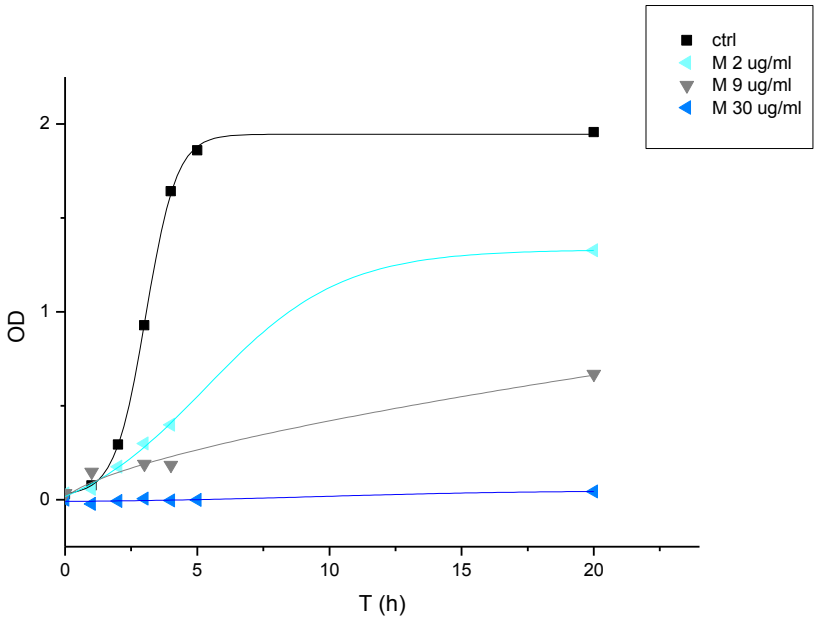

Figure 5.35 VCN-Loaded MZN inhibition test in TSB of *S. aureus* ATCC 6538. The black curve represents the negative control. Other curves show increasing concentrations of VCN-loaded MZNs. VCN content is about the 20% of the weight of NPs. The MIC of VCN-loaded MZNs (about 9 µg/ml) is obtained comparing these curves.

5.7 Inhibition tests on plate

The test on TSA gives a more immediate data than tests in TSB. Several concentrations both of bacteria and NPs were tested. These tests were conducted taking as reference the negative control of *S. aureus*, without antimicrobial agents, as shown in figure **5.36 A**. VCN inhibition tests against *S. aureus* confirm what reported in literature (Fig. **5.36 C** and **D**). Finally, figure **5.37** shows the four concentration chosen from all tested for these experiments. In respect of inhibition tests in TSB, these concentrations gave excellent results, comparing VCN-loaded MZNs and free VCN. Preliminary tests for VCN-loaded HAp-MZNs were conducted and, considering the same quantity of loaded drug, the loading efficiencies are comparable.

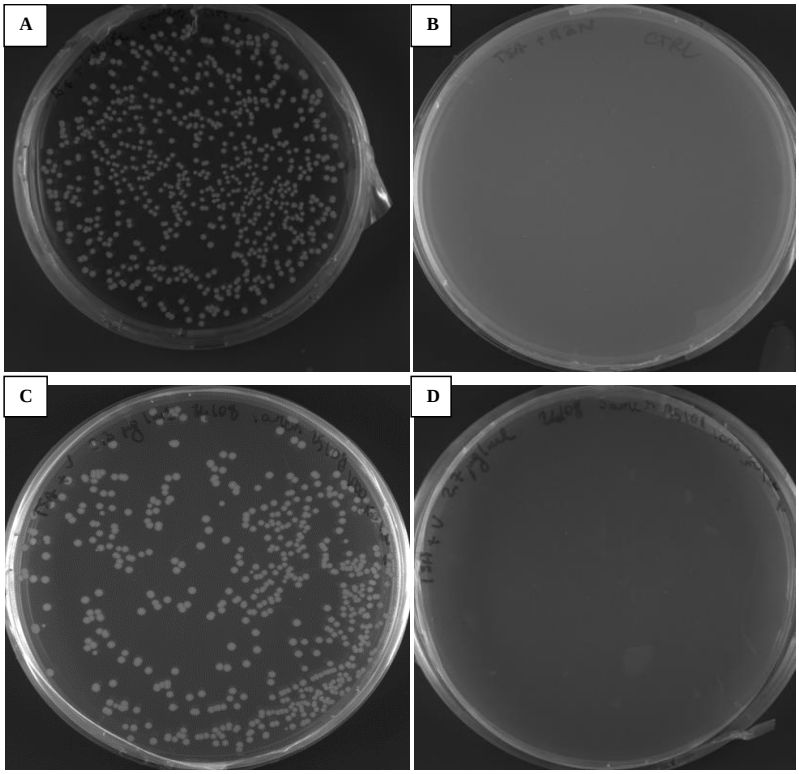

Figure 5.36 A: *S. aureus* ATCC 6538, negative control, without antimicrobial agents **B:** Contamination test shows the absence of contamination, because MZN inoculum doesn't give any bacterial colony. **C:** VCN inhibition test plate of *S. aureus*, VCN 0.3 µg/ml. **D:** VCN inhibition test plate of *S. aureus*, VCN 2.7 µg/ml.

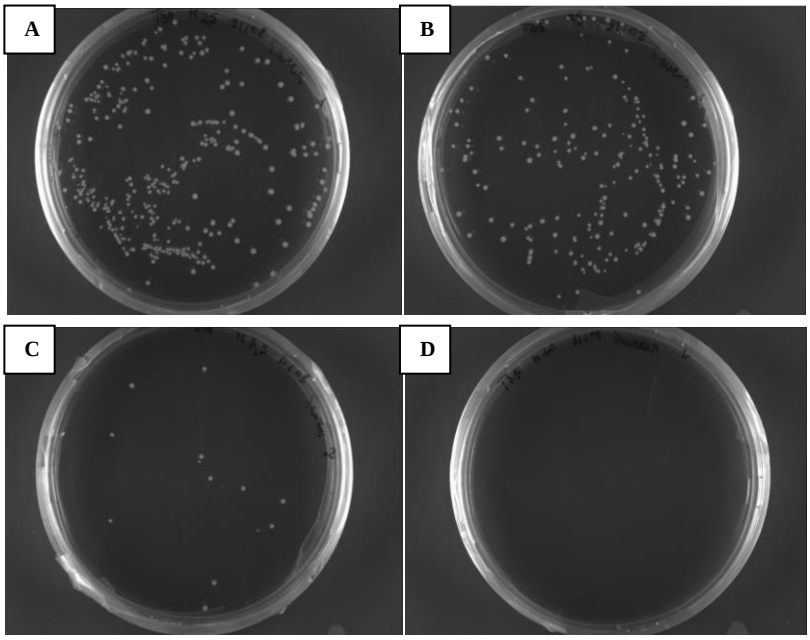

Figure 5.37 VCN-Loaded MZN inhibition test plates of *S. aureus* at increasing concentration. **A**: 2.5 µg/ml of MZNs, corresponding to 0.5 µg/ml of loaded VCN. **B**: 5 µg/ml of NPs corresponding to 1 µg/ml of VCN. **C**: 7.5 µg/ml of MZNs corresponding to 1.5 µg/ml of loaded VCN. **D**: 10 µg/ml of MZNs, corresponding to 2 µg/ml of VCN.

Figure **5.38** represents the inhibition tests of VCN-Loaded MZNs and the stability of this DDSs over the time, since the loading of the system. The green curve shows the viability curve of the bacterial strain with increasing concentrations of loaded-NPs. From fit data, the loaded MZN MIC was about 8.5 µg/ml ($IC_{50} \approx$ 5µg/ml). Taking into account the VCN content (about 20% w/w), the MIC value is about 1.7 µg/ml of drug. The black curve represents the same experiment after 15 days. As shown in the picture, MIC value increases to about 10.5 µg/ml ($IC_{50} \approx$ 8µg/ml). After 45 days from the loading of NPs, the highest used concentration of VCN-loaded NPs lost its biocidal effect. The MIC after this time is greatly increased. The reason could be the storage temperature of the DDS and the possible stress of the drug or the resistance of the strain to VCN. However, the stability of free drug is ensured for two weeks at room or refrigeration temperature of 4°C.

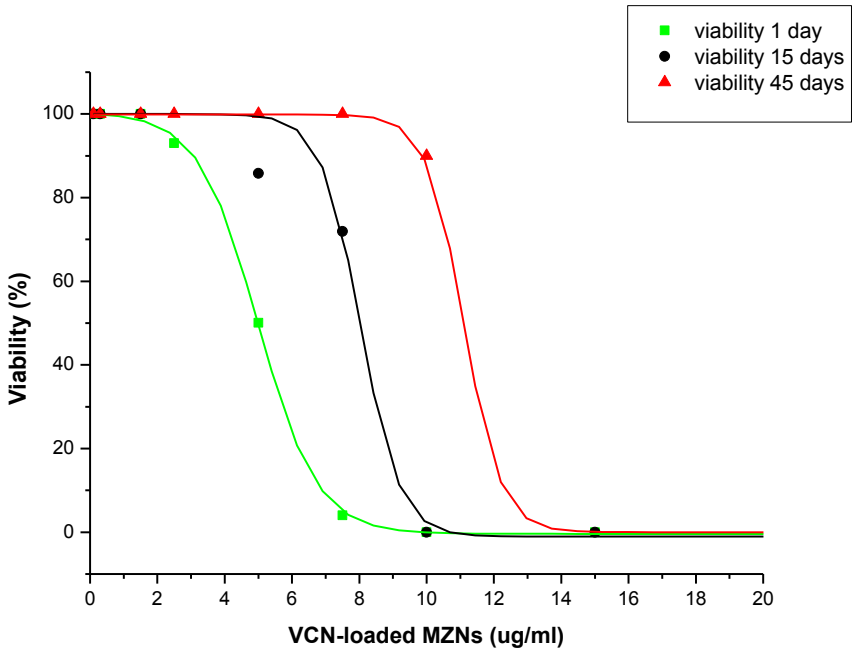

Figure 5.38 VCN-loaded MZN inhibition tests on plates during the time. The MIC values, found from the fit of the curves, significantly increase.

5.8 Biofilm inhibition/eradication tests

Calgary device is an useful instrument to test antimicrobial agents for biofilm inhibition or eradication. All kind of VCN-loaded NPs described in previous paragraphs were tested in both these experiments, as shown in figures **5.39** and **5.40**. MZNs without VCN are completely inert and don't have any antibiofouling effect. Free VCN have much lower efficiency than VCN-loaded NPs, as shown in figure **5.41**. The antibiotic has effect both in inhibition and in

eradication tests at very high concentrations, while VCN-loaded NPs have effects at very low values. In particular, VCN has MBC and MBEC of more than 1500 µg/ml. Since the VCN content in used batches is about the 20% of the MZN weight, the working VCN concentration in these experiments is about 2.4 and 2.8 µg/ml (see fig. **5.42**), a value hundreds of times smaller than free drug, as reported in table **5.3**.

The hypothesized mechanisms of action are two. The first one refers to the mechanical damage that MZNs cause to EPS coating and protecting bacteria, thus allowing VCN to bypass the barrier and to have its biocidal action. The second theory could be that VCN-loaded MZNs permeate the EPS barrier and release the drug next to bacteria. For this reason, not loaded MZNs and free VCN were mixed and tested together, in order to understand if the antibiofouling activity depends on the combined action of these two or if the loading step was necessary to the DDS activity. In effect, combined presence of MZNs and VCN results in a lower antibiofouling activity than VCN-loaded MZNs but a better biocidal activity than free VCN. This suggests that MZNs permeate and probably cause a mechanical damage to the bacterial biofilm, allowing VCN to act inside the EPS layer, possibly with a local release mechanism. However the loading step is crucial to exploit the full efficacy of the system. An experiment that can confirm this theory is testing non-porous NPs mixed with the drug. VCN-loaded HAp-MZN MBC and MBEC have a value of about 26 µg/ml. Considering VCN content into HAp-MZNs is about the half of that in MZNs, VCN-loaded HAp-MZNs and MZNs have the same activity (see table **5.3**, third and fourth columns).

In literature[75], so many theories are hypothesized to understand biofilm resistance to antibiotic therapies. Some authors explain the inefficacy of antimicrobial agents with a delay caused by EPS barrier. Others describe neutralization reactions and mechanisms of antibiotics by bacteria inside the biofilm structure. The presence of a DDS could avoid all these mechanisms, in addition to all properties of a carrier related to lower toxicity and adverse effects of drugs. It can facilitate the penetration of drug, even exploiting water flow channels or adhering to biofilm barrier, but also hiding the antibiotic from all enzymes, efflux pumps, etc that could inactivate it. MZNs as DDS could thus extend the concept of "selective toxicity" of Paul Ehrlich[32], referring to antimicrobial agents that aren't toxic for eukaryotic cells, being completely inert and not harmful.

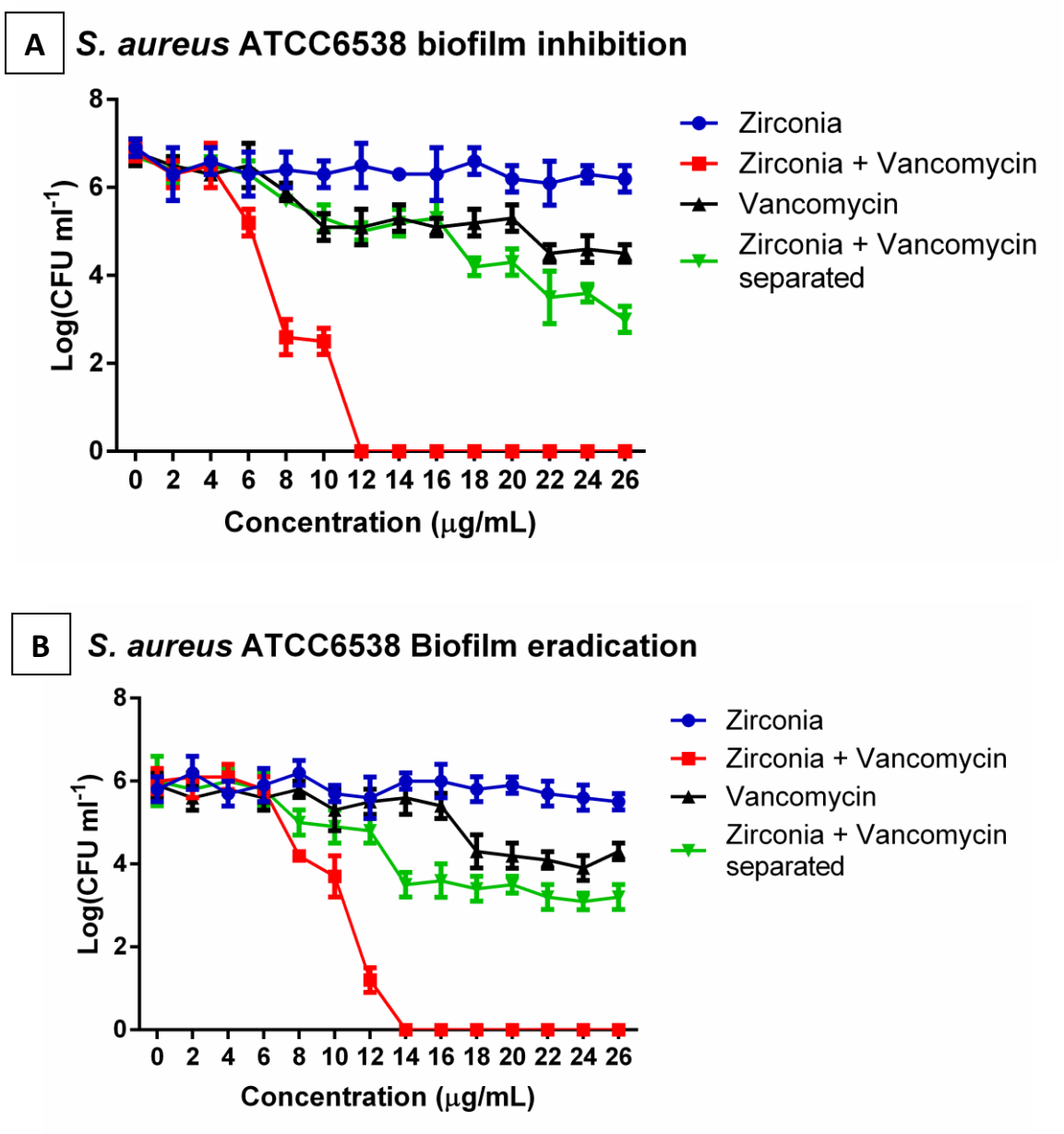

Figure 5.39 *S. aureus* biofilm inhibition **(A)** and eradication **(B)** tests. MZNs are completely inert, while VCN-loaded NPs work at a concentration of respectively 12 and 14 μg/ml, taking into account the actual VCN content of about 20% of their weight. Free VCN doesn't have effect at comparable concentration (see fig. **5.41**). The effectiveness of the loaded system is highlighted when Zirconia and VCN are separately tested in equal ratio. Comparing the results, the loaded system has greater activity than separated components.

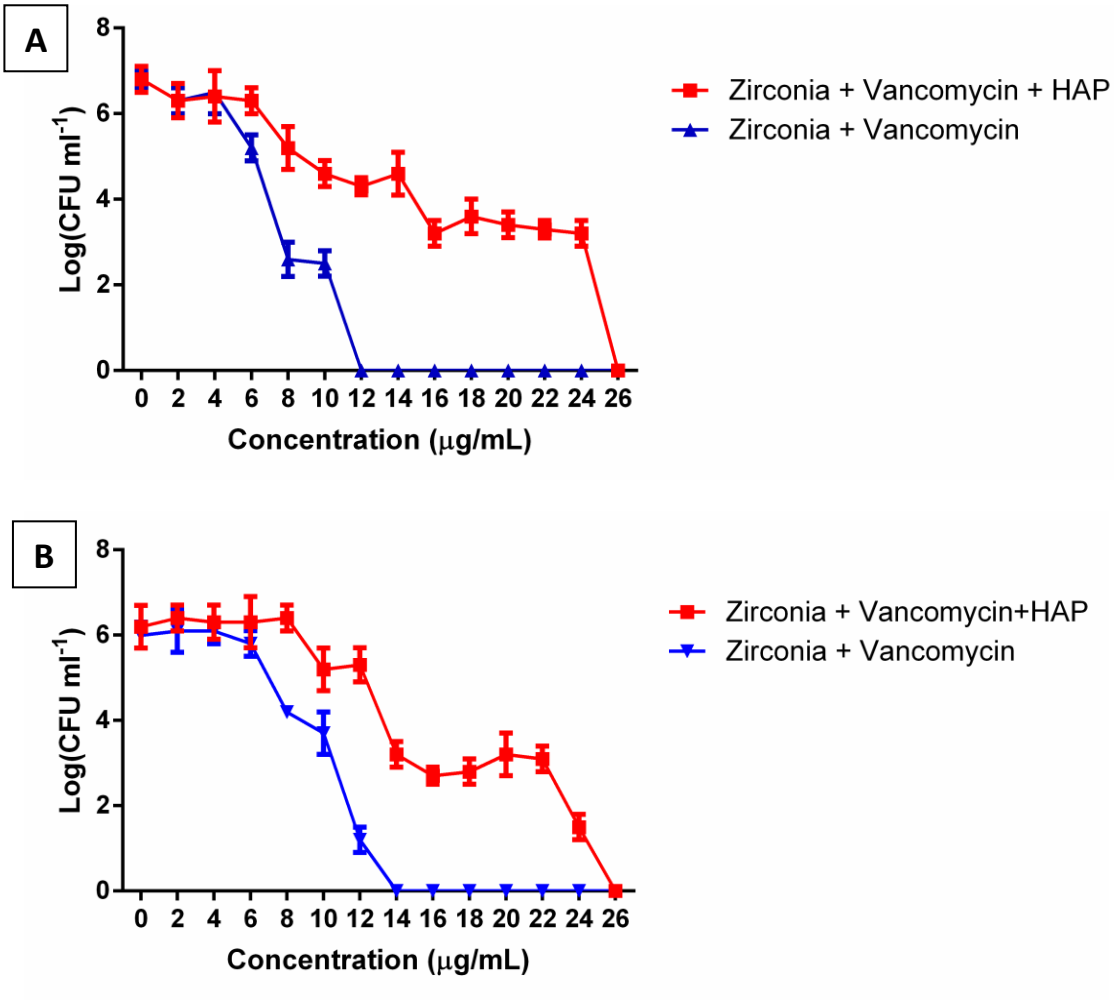

Figure 5.40 Biofilm inhibition **(A)** and **(B)** eradication tests comparison of VCN-loaded MZNs and VCN-loaded HAp-MZNs. Taking into account the loaded VCN amount, VCN-loaded HAp-MZNs and VCN-loaded MZNs have the same activity.

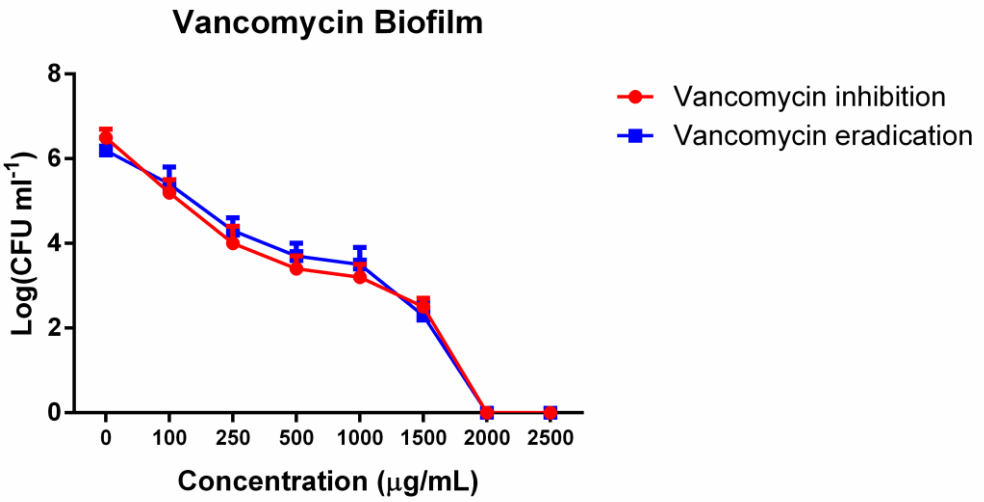

Figure 5.41 VCN inhibition/eradication tests against biofilm of *S. aureus*. The MBC and MBEC of free drug are greater than 1500 µg/ml.

Biofilm inhibition tests			
Tested agent	**DDS MBC (µg/ml)**	**Actual VCN content (µg/ml)**	**Loaded VCN (% w/w)**
MZNs	No activity	0	0
VCN-loaded MZNs	12	2.4	20
VCN-loaded HAp-MZNs	26	2.6	10
VCN	>1500	>1500	100
Biofilm eradication tests			
	DDS MBEC (µg/ml)	**Actual VCN content (µg/ml)**	**VCN loaded (% w/w)**
MZNs	No activity	0	0
VCN-loaded MZNs	14	2.8	20
VCN-loaded HAp-MZNs	26	2.6	10
VCN	>1500	>1500	100

Table 5.3 *S. aureus* biofilm inhibition and eradication tests. This table report s the results corresponding to loaded NPs and actual quantities of VCN inside them, expressed both in µg/ml and % of weight (third and fourth columns).

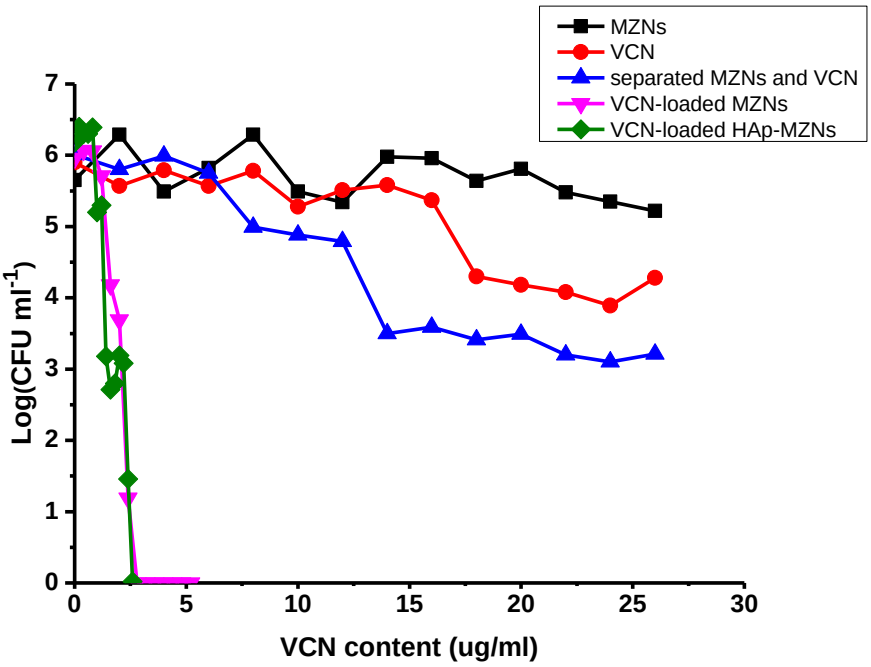

Figure 5.42 Biofilm eradication tests. Viability is function of VCN content inside NPs to compare the results with free drug effect to biofilm, making explicit the actual amount of drug used in the tests represented in fig. **5.39(B)**

5.9 Biofilm growth on glass coverslips for SEM and CLSM analyses

Another way to see and analyze bacterial biofilm can be microscopy. In this case, SEM and CLSM have been useful instruments to assess antibiofouling activity of this DDS. Adapting from Vuotto et al. protocol[69], biofilm of *S. aureus* were grown on glass cover slips in TSB + 1% glucose as shown in figure **5.43.**

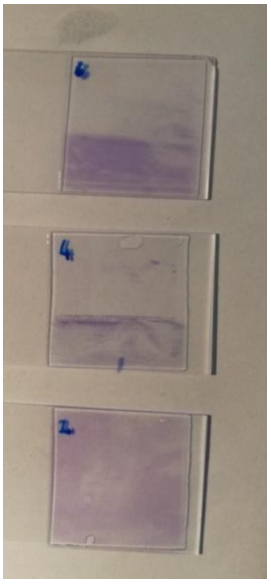

Figure 5.43 Biofilm of *S. aureus* ATCC 6538 on glass cover slips, marked with toluidine blue, not treated with DDSs.

Figure **5.44** shows FE-SEM images of *S. aureus* on cover slips not treated with antimicrobial agents. In addition to spherical bacterial cells, other material is visible around. It probably comes from cells broken during fixation and dehydration steps. On the background independent material is visible and it is probably the EPS matrix of biofilm.

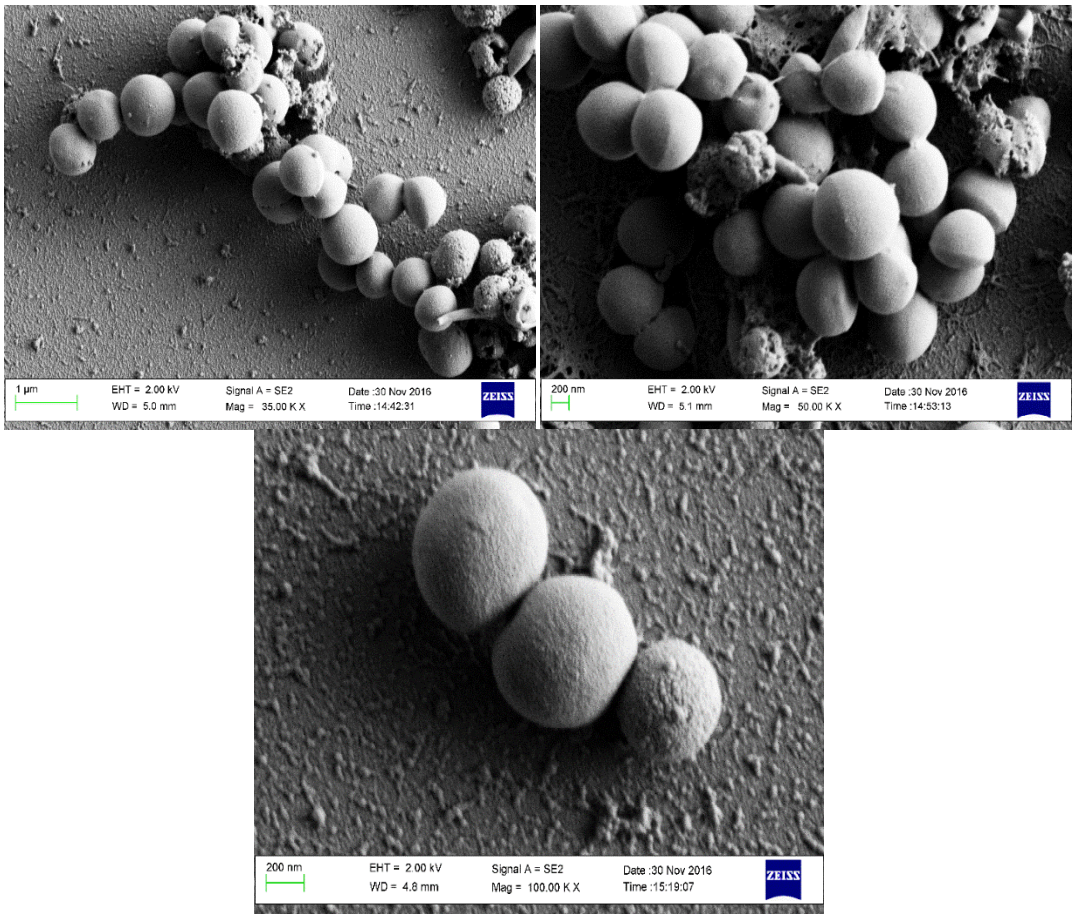

Figure 5.44 FEG-SEM images of biofilm of *Staphylococcus aureus* ATCC 6538. Pictures show the presence of typical *S. aureus* colonies and on the background the presence of a matrix, probably corresponding to biofilm EPS.

Figures **5.45** and **5.46** show CLSM images of untreated and treated biofilm of *S. aureus*. Biofilm EPSs are visible, giving red autofluorescence, probably for the treatment with glutaraldehyde to fix the biofilm on the glass cover slip. Bacterial cells are marked in blue with DAPI, that specifically binds the nucleus. Figure **5.45** shows untreated biofilm. Figure **5.46** shows treated biofilm with VCN-loaded MZNs and confirm the absence of biofilm matrix with the VCN-loaded NPs treatment.

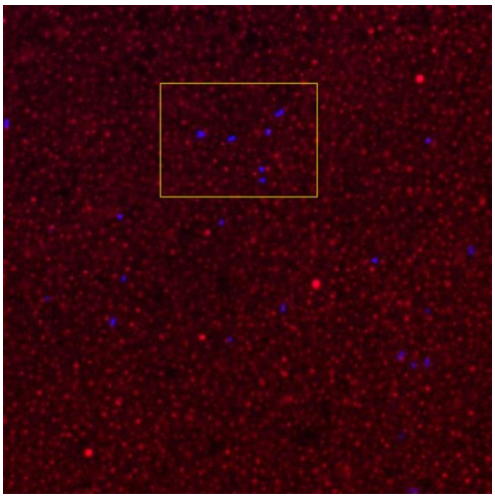

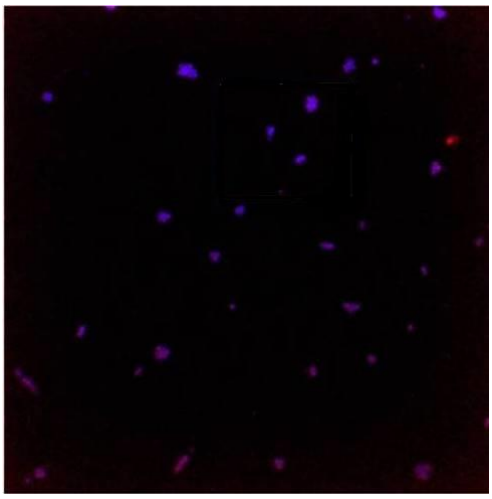

Figure 5.45 CLSM image of untreated *S. aureus* biofilm **Figure 5.46** CLSM image of treated biofilm of *S. aureus.* Untreated biofilm image shows the presence of an autofluorescent component, that probably corresponds to biofilm matrix.

Figure **5.47** shows treated biofilm of *S. aureus* and, in particular the possible interaction of NPs, represented by black dots, with bacteria. Consequence of this interaction is the release of drug next to NPs, improving its antibiofilm activity respect to free VCN. In addition to the mechanisms of action already mentioned in paragraph **5.8,** MZN could directly interact with bacterial cell wall due the high affinity of Zirconia and phosphate groups. The presence of teichoic acids (see fig. **1.6** and **1.8**) and other phosphate moieties could thus target MZNs to bacterial cells.

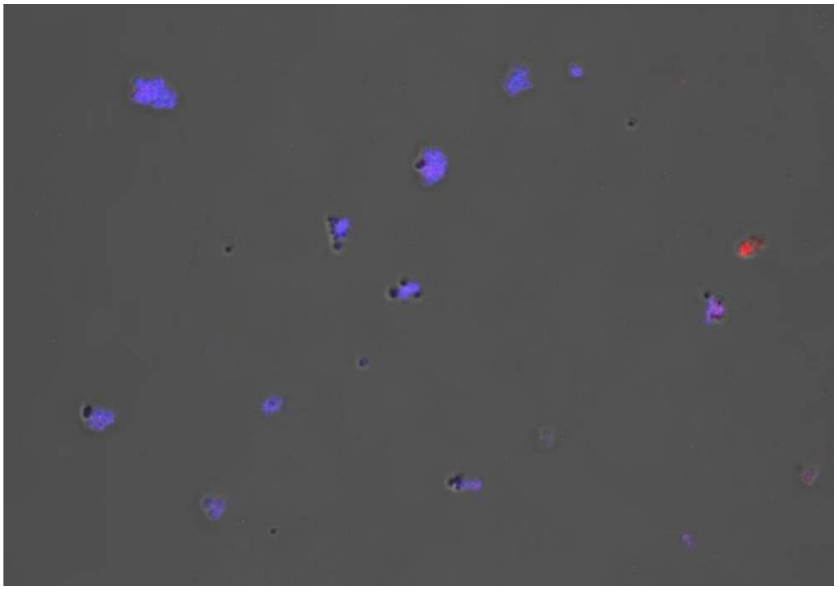

Figure 5.47 Bright field CLSM image of treated biofilm of *S. aureus.* Black dots probably represent VCN-loaded MZNs. The presence of exopolysaccharides of biofilm matrix is not detected.

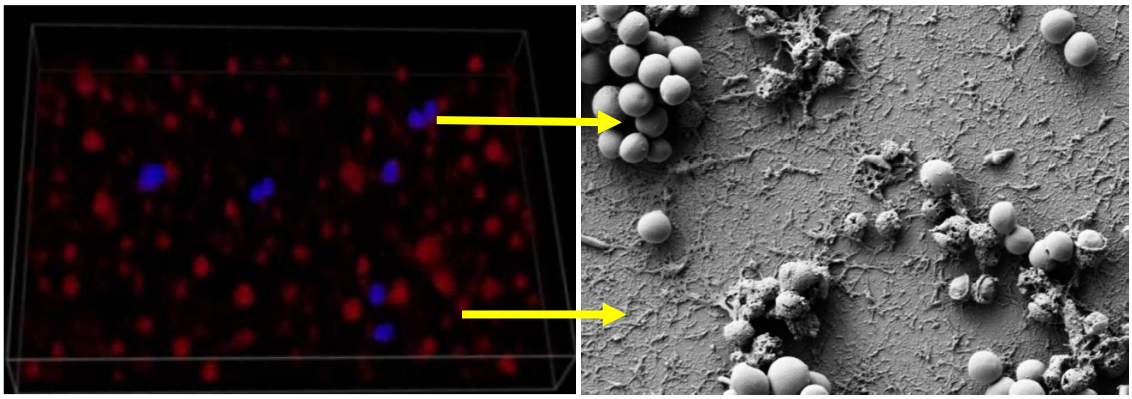

Figure 5.48 Comparison between CLSM (**on the left**) and SEM (**on the right**) images. These are two different representations of the same untreated biofilm of *S. aureus*. Blue bacterial cells marked in the first figure corresponds to the clusters of spherical cells in the second. The presence of EPS matrix is confirmed comparing the red autofluorescent component with material on the background of the second picture.

5.10 Preliminary studies on MSCs

All kind of cited NPs were marked with R6G and tested to assess a possible osteogenic activity towards progenitor cells of bone cells. HAp-MZNs and further functionalized HAp-MZNs with bis-phosphonate had best results, especially during first days of differentiation. Over the time, these NPs seem to have less activity against MSCs, compared to the control. These results could depend on the high size of NPs or on other functionalizations needed to conduct these experiments. For example, the phosphoascorbic acid could be interesting in culture medium, knowing about the great affinity of phosphate with zirconium oxide and about the strong impact that ascorbic acid has on MSC differentiation[76].

6 Conclusions and future perspectives

This work aimed to synthesize a DDS of VCN-loaded MZNs.

The different types of experiments performed showed that this DDS has improved properties than VCN alone. The lower efficacy of antibiotic against bacterial biofilms is a well known problem, reported also in literature. After confirming this effect, with this work we demonstrated that loaded NPs could be a successful instrument to overcome this limitation. As biofilms are one of the most relevant problem in medicine, in particular for nosocomial infections on biomedical devices, this DDS can be a practical solution for all cases of reimplantation of prosthesis caused by the presence of well-structured biofilm.

MZNs were also opportunely functionalized with HAp and a bis-phosphonate, becoming a promising instrument for tissue engineering and regenerative medicine, considering the complete bioinertia of zirconium oxide.

Future perspectives of this work regard further tests on biofilms: *in vitro*, on real prosthesis and, especially, *in vivo*, to validate the activity of loaded NPs also against mature biofilm.
Experiments on other bacterial species, such as Gram negative, or even fungal strains and their biofilm could be interesting to investigate and better understand the mechanism of action of loaded NPs. An experiment could be testing non-porous MZNs separated from the drug, to discriminate the actual role of NPs and the loading of the antibiotic to eradicate the biofilm. Other more detailed studies on the biofilm and NPs interactions with EDX-SEM and high resolution CLSM analyses could help in these cases. On the other hand, even the loading of MZNs with other antibiotics, also using appropriate functionalizations, could be important to generalize the technique.

About regenerative medicine, further experiments on MSCs should be conducted. For example, to improve MZNs as cell differentiation or cell growth promoters, further functionalizations with other molecules or further loading with other molecules or growth factors that can be useful as to promote these phenomena.

In this way, this work opened new fields of applications to mesoporous NPs and, especially, to zirconium(IV) oxide NPs, as microbiology and tissue regeneration.

7 Acknowledgments:

Thanks for the kind collaboration of prof. Alessandro Russo and Dr. Michele Bianchi of IOR of Bologna for CLSM images, Dr. Silvia Lampis and PhD Emanuele Zonaro of Department of Biotechnology of University of Verona for antibiofouling tests, PhD Maria Teresa Valenti of the Department of Medicine of University of Verona for preliminary tests on MSC cultures, Davide Cristofori for TEM analyses, Martina Marchiori for physisorption analyses, PhD Gabriele Sponchia and Riccardo Ottini for XRPD analyses.

8 Bibliography

1. Schimmel, T., Nanotechnology. An Introduction. By Jeremy J. Ramsden. *Angewandte Chemie International Edition* **2012,** *51* (39), 9733-9733.
2. Bawa, R.; Audette, G. F.; Rubinstein, I., *Handbook of Clinical Nanomedicine: Nanoparticles, Imaging, Therapy, and Clinical Applications*. Pan Stanford Publishing: 2016.
3. Filipponi, L.; Sutherland, D.; Center, I. N., NANOYOU teachers training kit in nanotechnologies. *European Commision Document, Denmark* **2010**.
4. Corbett, J.; McKeown, P.; Peggs, G.; Whatmore, R., Nanotechnology: international developments and emerging products. *CIRP Annals-Manufacturing Technology* **2000,** *49* (2), 523-545.
5. Chen, G.; Roy, I.; Yang, C.; Prasad, P. N., Nanochemistry and Nanomedicine for Nanoparticle-based Diagnostics and Therapy. *Chemical Reviews* **2016,** *116* (5), 2826-2885.
6. Raucci, M. G. Proprietà biologiche di materiali sintetizzati con la tecnica sol-gel. Università degli Studi di Napoli Federico II, 2006.
7. Di Bello, C., *Biomateriali: introduzione allo studio dei materiali per uso biomedico*. Pàtron: 2004.
8. Felice, B.; Prabhakaran, M. P.; Rodríguez, A. P.; Ramakrishna, S., Drug delivery vehicles on a nano-engineering perspective. *Materials Science and Engineering: C* **2014,** *41*, 178-195.
9. DURAN, N.; BOSIO, V. E.; FRATE, L.; CASTRO, G. R., Nanotechnology: Prospects and Perspectives.
10. Sponchia, G.; Ambrosi, E.; Rizzolio, F.; Hadla, M.; Del Tedesco, A.; Russo Spena, C.; Toffoli, G.; Riello, P.; Benedetti, A., Biocompatible tailored zirconia mesoporous nanoparticles with high surface area for theranostic applications. *J Mater Chem B* **2015,** *3* (36), 7300-7306.
11. Cales, B., Zirconia as a sliding material: histologic, laboratory, and clinical data. *Clinical orthopaedics and related research* **2000,** *379*, 94-112.
12. Piconi, C.; Maccauro, G., Zirconia as a ceramic biomaterial. *Biomaterials* **1999,** *20* (1), 1-25.
13. Ren, Z.; Zhang, G.; Chen, J. P., Adsorptive removal of arsenic from water by an iron–zirconium binary oxide adsorbent. *Journal of colloid and interface science* **2011,** *358* (1), 230-237.
14. Ren, Z.; Shao, L.; Zhang, G., Adsorption of phosphate from aqueous solution using an iron–zirconium binary oxide sorbent. *Water, Air, & Soil Pollution* **2012,** *223* (7), 4221-4231.
15. Long, F.; Gong, J.-L.; Zeng, G.-M.; Chen, L.; Wang, X.-Y.; Deng, J.-H.; Niu, Q.-Y.; Zhang, H.-Y.; Zhang, X.-R., Removal of phosphate from aqueous solution by magnetic Fe–Zr binary oxide. *Chem Eng J* **2011,** *171* (2), 448-455.
16. Liu, H.; Sun, X.; Yin, C.; Hu, C., Removal of phosphate by mesoporous ZrO2. *J Hazard Mater* **2008,** *151* (2–3), 616-622.
17. Yin, T.; Li, H.; Yang, N.; Gao, T.; Sun, L.; Li, G., Detection of CREB phosphorylation via Zr (IV) ion mediated signal amplification. *Biosensors and Bioelectronics* **2014,** *56*, 1-5.
18. Cinier, M.; Petit, M.; Williams, M. N.; Fabre, R. M.; Pecorari, F.; Talham, D. R.; Bujoli, B.; Tellier, C., Bisphosphonate adaptors for specific protein binding on zirconium phosphonate-based microarrays. *Bioconjugate Chem* **2009,** *20* (12), 2270-2277.
19. Kumar, S.; Kumar, S.; Tiwari, S.; Srivastava, S.; Srivastava, M.; Yadav, B. K.; Kumar, S.; Tran, T. T.; Dewan, A. K.; Mulchandani, A., Biofunctionalized nanostructured zirconia for biomedical application: a smart approach for oral cancer detection. *Advanced Science* **2015,** *2* (8).
20. Jangra, S. L.; Stalin, K.; Dilbaghi, N.; Kumar, S.; Tawale, J.; Singh, S. P.; Pasricha, R., Antimicrobial activity of zirconia (ZrO2) nanoparticles and zirconium complexes. *Journal of nanoscience and nanotechnology* **2012,** *12* (9), 7105-7112.
21. Gowri, S.; Gandhi, R. R.; Sundrarajan, M., Structural, optical, antibacterial and antifungal properties of zirconia nanoparticles by biobased protocol. *Journal of Materials Science & Technology* **2014,** *30* (8), 782-790.
22. Pal, S.; Tak, Y. K.; Song, J. M., Does the antibacterial activity of silver nanoparticles depend on the shape of the nanoparticle? A study of the gram-negative bacterium Escherichia coli. *Applied and environmental microbiology* **2007,** *73* (6), 1712-1720.

23. Wang, X.; Chen, D.; Cao, L.; Li, Y.; Boyd, B. J.; Caruso, R. A., Mesoporous Titanium Zirconium Oxide Nanospheres with Potential for Drug Delivery Applications. *Acs Appl Mater Inter* **2013,** *5* (21), 10926-10932.
24. Tang, S.; Huang, X.; Chen, X.; Zheng, N., Hollow mesoporous zirconia nanocapsules for drug delivery. *Advanced Functional Materials* **2010,** *20* (15), 2442-2447.
25. Katti, K. S., Biomaterials in total joint replacement. *Colloids and Surfaces B: Biointerfaces* **2004,** *39* (3), 133-142.
26. Earl, J.; Wood, D.; Milne, S. In *Hydrothermal synthesis of hydroxyapatite*, Journal of Physics: Conference Series, IOP Publishing: 2006; p 268.
27. Chen, W.; Long, T.; Guo, Y.-J.; Zhu, Z.-A.; Guo, Y.-P., Hydrothermal synthesis of hydroxyapatite coatings with oriented nanorod arrays. *Rsc Adv* **2014,** *4* (1), 185-191.
28. Wang, Y.; Zhang, S.; Wei, K.; Zhao, N.; Chen, J.; Wang, X., Hydrothermal synthesis of hydroxyapatite nanopowders using cationic surfactant as a template. *Materials Letters* **2006,** *60* (12), 1484-1487.
29. Lu, H.; Liu, Y.; Guo, J.; Wu, H.; Wang, J.; Wu, G., Biomaterials with Antibacterial and Osteoinductive Properties to Repair Infected Bone Defects. *International journal of molecular sciences* **2016,** *17* (3), 334.
30. Sakai, Y.; Qin, L.; Miura, M.; Masunaga, K.; Tanamachi, C.; Iwahashi, J.; Kida, Y.; Takasu, O.; Sakamoto, T.; Watanabe, H., Successful infection control for a vancomycin-intermediate Staphylococcus aureus outbreak in an advanced emergency medical service centre. *Journal of Hospital Infection* **2016,** *92* (4), 385-391.
31. Inweregbu, K.; Dave, J.; Pittard, A., Nosocomial infections. *Continuing Education in Anaesthesia, Critical Care & Pain* **2005,** *5* (1), 14-17.
32. Madigan, M. T.; Brock, T. D.; Baldi, F., *Brock. Biologia dei microrganismi*. Pearson: 2012.
33. Martinez, L. R.; Han, G.; Chacko, M.; Mihu, M. R.; Jacobson, M.; Gialanella, P.; Friedman, A. J.; Nosanchuk, J. D.; Friedman, J. M., Antimicrobial and healing efficacy of sustained release nitric oxide nanoparticles against Staphylococcus aureus skin infection. *Journal of Investigative Dermatology* **2009,** *129* (10), 2463-2469.
34. Tong, S. Y.; Davis, J. S.; Eichenberger, E.; Holland, T. L.; Fowler, V. G., Staphylococcus aureus infections: epidemiology, pathophysiology, clinical manifestations, and management. *Clinical microbiology reviews* **2015,** *28* (3), 603-661.
35. Chambers, H. F.; DeLeo, F. R., Waves of resistance: Staphylococcus aureus in the antibiotic era. *Nature Reviews Microbiology* **2009,** *7* (9), 629-641.
36. Pace, J. L.; Rupp, M. E.; Finch, R. G., *Biofilms, infection, and antimicrobial therapy*. CRC Press: 2005.
37. Hammes, W. P.; Neuhaus, F. C., On the mechanism of action of vancomycin: inhibition of peptidoglycan synthesis in Gaffkya homari. *Antimicrobial agents and chemotherapy* **1974,** *6* (6), 722-728.
38. Nagarajan, R., *Glycopeptide antibiotics*. CRC Press: 1994; Vol. 63.
39. Nicolosi, D.; Scalia, M.; Nicolosi, V. M.; Pignatello, R., Encapsulation in fusogenic liposomes broadens the spectrum of action of vancomycin against Gram-negative bacteria. *International journal of antimicrobial agents* **2010,** *35* (6), 553-558.
40. Gardete, S.; Tomasz, A., Mechanisms of vancomycin resistance in Staphylococcus aureus. *The Journal of clinical investigation* **2014,** *124* (7), 2836-2840.
41. Hazlewood, K. A.; Brouse, S. D.; Pitcher, W. D.; Hall, R. G., Vancomycin-associated nephrotoxicity: grave concern or death by character assassination? *The American journal of medicine* **2010,** *123* (2), 182. e1-182. e7.
42. Bailie, G. R.; Neal, D., Vancomycin ototoxicity and nephrotoxicity. *Medical toxicology and adverse drug experience* **1988,** *3* (5), 376-386.
43. Kurczewska, J.; Sawicka, P.; Ratajczak, M.; Gajęcka, M.; Schroeder, G., Vancomycin-modified silica: Synthesis, controlled release and biological activity of the drug. *Int J Pharmaceut* **2015,** *486* (1), 226-231.
44. Gu, J.; Wang, T.; Fan, G.; Ma, J.; Hu, W.; Cai, X., Biocompatibility of artificial bone based on vancomycin loaded mesoporous silica nanoparticles and calcium sulfate composites. *Journal of Materials Science: Materials in Medicine* **2016,** *27* (4), 1-11.

45. Li, H.; Gu, J.; Shah, L. A.; Siddiq, M.; Hu, J.; Cai, X.; Yang, D., Bone cement based on vancomycin loaded mesoporous silica nanoparticle and calcium sulfate composites. *Materials Science and Engineering: C* **2015,** *49*, 210-216.
46. Loca, D.; Sokolova, M.; Locs, J.; Smirnova, A.; Irbe, Z., Calcium phosphate bone cements for local vancomycin delivery. *Materials Science and Engineering: C* **2015,** *49*, 106-113.
47. Stigter, M.; Bezemer, J.; De Groot, K.; Layrolle, P., Incorporation of different antibiotics into carbonated hydroxyapatite coatings on titanium implants, release and antibiotic efficacy. *Journal of controlled release* **2004,** *99* (1), 127-137.
48. Suchý, T.; Šupová, M.; Klapková, E.; Horný, L.; Rýglová, Š.; Žaloudková, M.; Braun, M.; Sucharda, Z.; Ballay, R.; Veselý, J., The Sustainable Release of Vancomycin and Its Degradation Products From Nanostructured Collagen/Hydroxyapatite Composite Layers. *Journal of pharmaceutical sciences* **2016,** *105* (3), 1288-1294.
49. (a) Ueng, S. W.; Lin, S.-S.; Wang, I.-C.; Yang, C.-Y.; Cheng, R.-C.; Liu, S.-J.; Chan, E.-C.; Lai, C.-F.; Yuan, L.-J.; Chan, S.-C., Efficacy of vancomycin-releasing biodegradable poly (lactide-co-glycolide) antibiotics beads for treatment of experimental bone infection due to Staphylococcus aureus. *Journal of orthopaedic surgery and research* **2016,** *11* (1), 1; (b) Zakeri-Milani, P.; Loveymi, B. D.; Jelvehgari, M.; Valizadeh, H., The characteristics and improved intestinal permeability of vancomycin PLGA-nanoparticles as colloidal drug delivery system. *Colloids and Surfaces B: Biointerfaces* **2013,** *103*, 174-181.
50. Posadowska, U.; Brzychczy-Wloch, M.; Pamula, E., Injectable gellan gum-based nanoparticles-loaded system for the local delivery of vancomycin in osteomyelitis treatment. *Journal of Materials Science: Materials in Medicine* **2016,** *27* (1), 1-9.
51. Szász, M.; Hajdú, M.; Pesti, N.; Domahidy, M.; Kristóf, K.; Zahár, á.; Nagy, K.; Szabó, D., In vitro efficiency of vancomycin containing experimental drug delivery systems. *Acta microbiologica et immunologica Hungarica* **2013,** *60* (4), 461-468.
52. Lian, X.; Liu, H.; Wang, X.; Xu, S.; Cui, F.; Bai, X., Antibacterial and biocompatible properties of vancomycin-loaded nano-hydroxyapatite/collagen/poly (lactic acid) bone substitute. *Progress in Natural Science: Materials International* **2013,** *23* (6), 549-556.
53. Darouiche, R. O.; Dhir, A.; Miller, A. J.; Landon, G. C.; Raad, I. I.; Musher, D. M., Vancomycin penetration into biofilm covering infected prostheses and effect on bacteria. *Journal of Infectious Diseases* **1994,** *170* (3), 720-723.
54. Badri, M.; Zawaneh, S.; Cruz, A., Vancomycin Penetration into Biofilm Covering Infected Prostheses and Effect on Bacteria. *Infect Dis* **1977,** *135*, 308-12.
55. Tomás, I.; Henderson, B.; Diz, P.; Donos, N., In vivo oral biofilm analysis by confocal laser scanning microscopy: methodological approaches. *Microscopy Science, technology, applications and education. Badajoz (Spain): Formatex* **2010**, 597-606.
56. Cogan, N.; Cortez, R.; Fauci, L., Modeling physiological resistance in bacterial biofilms. *Bulletin of mathematical biology* **2005,** *67* (4), 831-853.
57. Wixtrom, R. N.; Stutman, R. L.; Burke, R. M.; Mahoney, A. K.; Codner, M. A., Risk of breast implant bacterial contamination from endogenous breast flora, prevention with nipple shields, and implications for biofilm formation. *Aesthetic Surgery Journal* **2012,** *32* (8), 956-963.
58. Valenti, M. T.; Mori, A.; Malerba, G.; Dalle Carbonare, L., Mesenchymal stem cells: A new diagnostic tool? *World journal of stem cells* **2015,** *7* (5), 789.
59. Peterson, S. B.; Irie, Y.; Borlee, B. R.; Murakami, K.; Harrison, J. J.; Colvin, K. M.; Parsek, M. R., Different methods for culturing biofilms in vitro. In *Biofilm Infections*, Springer: 2011; pp 251-266.
60. Harrison, J. J.; Stremick, C. A.; Turner, R. J.; Allan, N. D.; Olson, M. E.; Ceri, H., Microtiter susceptibility testing of microbes growing on peg lids: a miniaturized biofilm model for high-throughput screening. *Nature protocols* **2010,** *5* (7), 1236-1254.
61. Jorgensen, T. M.; Haagensen, J.; Sternberg, C.; Molin, S., Quantification of biofilm structure from confocal imaging. *Visionday 2003 of Technical University of Dinmark* **2003**.
62. Zonaro, E.; Lampis, S.; Turner, R. J.; Qazi, S. J. S.; Vallini, G., Biogenic selenium and tellurium nanoparticles synthesized by environmental microbial isolates efficaciously inhibit bacterial planktonic cultures and biofilms. *Frontiers in microbiology* **2015,** *6*.
63. Mu, H.; Tang, J.; Liu, Q.; Sun, C.; Wang, T.; Duan, J., Potent Antibacterial Nanoparticles against Biofilm and Intracellular Bacteria. *Scientific reports* **2016,** *6*.

64. Hajipour, M. J.; Fromm, K. M.; Ashkarran, A. A.; de Aberasturi, D. J.; de Larramendi, I. R.; Rojo, T.; Serpooshan, V.; Parak, W. J.; Mahmoudi, M., Antibacterial properties of nanoparticles. *Trends in biotechnology* **2012,** *30* (10), 499-511.
65. Smith, A. W., Biofilms and antibiotic therapy: is there a role for combating bacterial resistance by the use of novel drug delivery systems? *Advanced drug delivery reviews* **2005,** *57* (10), 1539-1550.
66. Chakraborty, S. P.; Sahu, S. K.; Pramanik, P.; Roy, S., In vitro antimicrobial activity of nanoconjugated vancomycin against drug resistant Staphylococcus aureus. *Int J Pharmaceut* **2012,** *436* (1), 659-676.
67. Forier, K.; Raemdonck, K.; De Smedt, S. C.; Demeester, J.; Coenye, T.; Braeckmans, K., Lipid and polymer nanoparticles for drug delivery to bacterial biofilms. *Journal of Controlled Release* **2014,** *190*, 607-623.
68. Hermanson, G. T., *Bioconjugate Techniques*. Elsevier Science: 2013.
69. Vuotto, C.; Donelli, G., Field Emission Scanning Electron Microscopy of Biofilm-Growing Bacteria Involved in Nosocomial Infections. *Microbial Biofilms: Methods and Protocols* **2014**, 73-84.
70. Brinker, C. J.; Scherer, G. W., *Sol-gel science: the physics and chemistry of sol-gel processing*. Academic press: 2013.
71. Dapiaggi, M.; Maglia, F.; Tredici, I.; Maroni, B.; Borghini, G.; Tamburini, U. A., Complex thermal evolution of size-stabilized tetragonal zirconia. *J Phys Chem Solids* **2010,** *71* (8), 1038-1041.
72. Carter, C. B.; Williams, D. B., *Transmission electron microscopy*. Springer-Verlag US: 2009.
73. Takács-Novák, K.; Noszál, B.; Tókés-Kövesdi, M.; Szász, G., Acid-base properties and proton-speciation of vancomycin. *Int J Pharmaceut* **1993,** *89* (3), 261-263.
74. Dash, S.; Murthy, P. N.; Nath, L.; Chowdhury, P., Kinetic modeling on drug release from controlled drug delivery systems. *Acta Pol Pharm* **2010,** *67* (3), 217-23.
75. Xiong, M.-H.; Bao, Y.; Yang, X.-Z.; Zhu, Y.-H.; Wang, J., Delivery of antibiotics with polymeric particles. *Advanced drug delivery reviews* **2014,** *78*, 63-76.
76. Fiorentini, E. Modulazione del differenziamento osteogenico di precursori mesenchimali umani per applicazioni di ingegneria tissutale. alma, 2012.